REPORT SERIES IN AEROSOL SCIENCE
N:o 158 (2014)

# REMOTE SENSING OF AEROSOLS: APPLICATIONS FOR AIR QUALITY AND CLIMATE STUDIES

ANU-MAIJA SUNDSTRÖM

Division of Atmospheric Sciences
Department of Physics
Faculty of Science
University of Helsinki
Helsinki, Finland

Academic dissertation

*To be presented, with the permission of the Faculty of Science of the University of Helsinki for public criticism in Exactum auditorium CK112, Gustaf Hällströmin katu 2, on December 10th, 2014, at 12 o'clock noon.*

**Helsinki 2014**

Author's Address: Department of Physics
P.O. Box 64, FI-00014 University of Helsinki
anu-maija.sundstrom@helsinki.fi

Supervisors: Professor Markku Kulmala, Ph.D.
Department of Physics, University of Helsinki

Professor Gerrit de Leeuw, Ph.D.
Department of Physics, University of Helsinki, and
Finnish Meteorological Institute

Senior Researcher Timo Nousiainen, Ph.D.
Finnish Meteorological Institute

Senior Scientist Antti Arola, Ph.D.
Finnish Meteorological Institute

Reviewers: Research Professor Jouni Pulliainen, Ph.D.
Arctic Research Centre, Finnish Meteorological Institute

Associate Professor Ilona Riipinen, Ph.D.
Department of Applied Environmental Science
University of Stockholm

Opponent: Senior Scientist Michael Schulz, Ph.D.
Climate and Air pollution Section
Norwegian Meteorological Institute

ISBN 978-952-7091-08-1 (printed version)
ISSN 0784-3496
Helsinki 2014
Unigrafia Oy

ISBN 978-952-7091-09-8 (pdf version)
http://ethesis.helsinki.fi
Helsinki 2014
Helsingin yliopiston verkkojulkaisut

## Acknowledgements

The research presented in this thesis has been carried out at the Department of Physics, University of Helsinki. The head of the department until 2013, Prof. Juhani Keinonen, and since that Prof. Hannu Koskinen are acknowledged for providing the work facilities.

I am first and foremost thankful to my supervisors Prof. Markku Kulmala, Prof. Gerrit de Leeuw, Dr. Timo Nousiainen, and Dr. Antti Arola for the guidance during this PhD work. I'm grateful that I've had the opportunity to work with remote sensing from so many different aspects.

This work would not have been possible without the collaboration with my colleagues and co-authors. Particularly I would like to thank the Remote Sensing Group at the University of Helsinki and at the Finnish Meteorological Institute: Larisa Sogacheva, Pekka Kolmonen, Timo Virtanen, Edith Rodriguez, Ksenia Atlaskina, Anna Nikandrova, Giulia Saponaro, and Sini Merikallio. I also thank all the unique people at the Division of Atmospheric Sciences, and at the Finnish Meteorological Institute, both in Helsinki and in Kuopio, for the good scientific collaboration, conversations, ideas and advices.

Being able to attend international conferences and workshops during these years has had a large impact on my work. In addition to the Division of Atmospheric Sciences, I would like to acknowledge the Väisälä Foundation, Chancellor's travel grant (University of Helsinki), Gordon Research Conferences, and Suomalainen Konkordialiitto for the additional financial support for the travel. I would also like to acknowledge the numerous people from Vaisala Oyj, the National Aeronautics and Space Administration, and the European Space Agency, who have helped me with the technical questions related to the remote sensing data used in this work.

Last but not least I owe my gratitude to my family, for the support and encouragement they have given me throughout these years.

Anu-Maija Sundström
University of Helsinki, 2014

**Abstract**

Atmospheric aerosol particles affect public health, environment, weather and climate in various ways, and therefore the importance on obtaining information about their spatial and temporal variation is evident. Remote sensing measurements have particular capability to provide broad horizontal and/or vertical view on the ambient aerosol field from local to global scales. They also can provide observations over remote areas where carrying out in situ measurements is not possible. The aim of this Thesis, is to explore both ground-based and spaceborne remote sensing measurement techniques for monitoring aerosol particles, and their applications on air quality as well as climate studies.

In the first part of this Thesis the potential of a ground-based ceilometer-type lidar to be used as an aerosol measurement device is investigated. Ceilometers are originally designed for observing cloud heights, and at the time of the study they were not commonly used to monitor aerosols. The results obtained in this study indicate that the absolute accuracy of a ceilometer-type lidar is sufficient for quantitative aerosol measurements in some applications.

The first study using an improved version of the AATSR (Advanced Along-Track Scanning Radiometer) satellite algorithm shows that aerosol optical depth (AOD) can be retrieved with sufficient accuracy over Eastern China, where the aerosol conditions are highly variable and therefore challenging from the satellite remote sensing point of view. In addition, the improved version of the algorithm provides also valuable information about the fine mode particle contribution to the total AOD. The satellite based AOD data is also used to evaluate the performance of a coupled climate-aerosol model. The comparison of ECHAM5-HAM model and satellite-based AOD (from MODerate Imaging Spectroradiometer) showed that, with few exceptions, the model reproduced relatively well the spatiotemporal variation of AOD over India and China.

In this Thesis it is also shown that satellite data can be used to derive such climatically relevant quantities that are not directly available in common retrieval products (such as e.g. AOD). By combining coincident observations from two different satellite instruments, an observation-based estimate of the clear-sky shortwave aerosol direct radiative effect ADRE (at the top of the atmosphere) can be established. Results of the case study over Eastern China show that, overall, the satellite-based estimates of ADRE, aerosol-free fluxes, and their spatial variation are in agreement with model-based values.

Keywords: aerosol remote sensing, aerosol optical depth, aerosol direct radiative effect.

# Contents

## List of publications

This Thesis consists of an introductory review, followed by four research articles. In the introductory part, these papers are cited according to their roman numerals. Paper **I** is reproduced with permission from the American Meteorological Society. Papers **II-IV** are reproduced under the Creative Common Attribution Licence.

**I** Sundström, A.-M., Nousiainen, T., and Petäjä, T. (2009). On the Quantitative Low-Level Aerosol Measurements Using Ceilometer-Type Lidar, *J. Atmos. Oceanic Technol.*, 26: 2340–2352.

**II** Sundström, A.-M., Kolmonen, P., Sogacheva, L., and de Leeuw, G. (2012). Aerosol retrievals over China with the AATSR dual view algorithm, *Remote Sens. Environ.*, 116: 189–198.

**III** Henriksson, S. V., Laaksonen, A., Kerminen, V-M., Räisänen, P., Järvinen, H., Sundström, A-M., and de Leeuw, G. (2011). Spatial distributions and seasonal cycles of aerosols in India and China seen in global climate-aerosol model. *Atmos. Chem. Phys.*, 11: 7975–7990.

**IV** Sundström, A.-M., Arola, A., Kolmonen, P., Xue, Y., de Leeuw, G., and Kulmala, M. (2014). On the use of satellite remote sensing based approach for determining aerosol direct radiative effect over land: a case study over China, *Atmos. Chem. Phys. Discuss.*, 14: 15113–15147. Accepted for publication in *Atmos. Chem. Phys.*.

# 1 Introduction

Atmospheric aerosol particles are one of the central topics in current environmental research due to their various effects on atmospheric physics and chemistry, biosphere, public health and climate. This Thesis explores both ground-based and spaceborne remote sensing methods for monitoring atmospheric aerosol particles, their effects on air quality and climate.

An aerosol is defined as a disperse system of a solid or liquid particles suspended in a carrier gas. The tiny solid or liquid particles that are suspended in the air are referred to as atmospheric aerosol particles. It is also common to use the term aerosol to refer to only the solid or liquid particles and exclude the carrier gas. Aerosol particles can be divided into two categories by their origin. Primary particles are emitted directly in solid or liquid form into the atmosphere. Two major natural sources of primary aerosol particles are deserts and oceans, where wind-driven dust particles from the soil or sea salt from bursting bubbles are emitted directly into the air, while diesel engines and combustion processes are among the man-made sources of primary particles. Secondary particles are formed from some precursor gas via gas-to-particle conversion, often referred to as "new particle formation" (NPF) or nucleation. Several field studies have shown that nucleation occurs frequently in the atmosphere in a variety of environments; in clean Antarctica (Kyrö et al., 2013), boreal forests (e.g. Mäkelä et al., 2000; Dal Maso et al., 2005), as well as semi-clean (e.g. Vakkari et al., 2011) and polluted areas (e.g. Wang et al., 2013; Kanawade et al., 2014). The main constituents of atmospheric aerosol particles are inorganic and organic species, black carbon, minerals, and primary biological particles.

Aerosol particles are often classified by their diameter $D_p$, which can vary from a few nanometers to hundreds of micrometers. The newly formed particles are often referred as nucleation mode particles and their diameters range from few to ten nanometers. Particles in the size range of 10 nm $< D_p <$100 nm are referred to Aitken mode particles, and particles 100 nm $< D_p < 1$ $\mu$m as accumulation mode particles. Coarse mode particles are typically defined as $D_p > 1$ $\mu$m. The other widely used size-related classification of aerosols is to divide them into $PM_{2.5}$ and $PM_{10}$ particles. The fine $PM_{2.5}$ particles include aerosols with $D_p < 2.5$ $\mu$m, whereas for $PM_{10}$ $D_p < 10$ $\mu$m. Once formed or emitted in the atmosphere, aerosols undergo various physical processes and chemical interactions (Fig. 1).

Most often aerosol particles are concentrated in the lowest atmospheric layer that is in direct interaction with the Earth's surface, often referred as the atmospheric boundary layer, which can vary in depth from few meters to several kilometres depending on the meteorological conditions. Typically in the marine boundary layer the aerosol particle number concentration vary between 300-2000 $cm^{-3}$ and in the continental boundary layer between 1000-10000 $cm^{-3}$ (Spracklen et al., 2010). While suspended in the air, aerosol particles can be transported to

significant distances from their sources. The residence time of aerosol particles varies typically from a few days to weeks, depending on the aerosol particle type and on meteorological conditions.

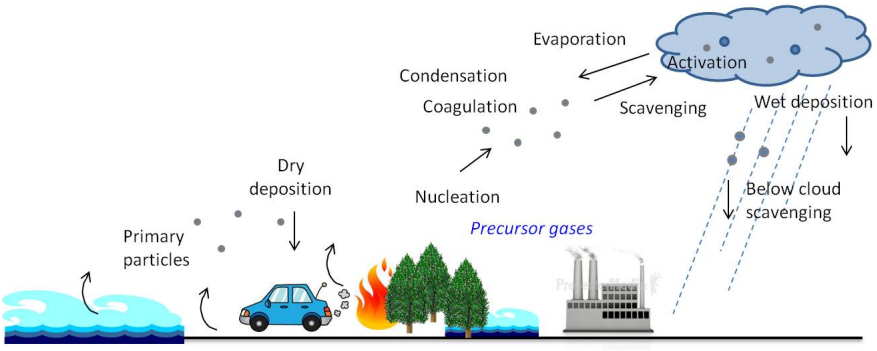


Figure 1: Schematic illustration of various processes that aerosols undergo in the atmosphere.

The importance of studying aerosol particles relates to their immediate and long-term effects on public health and the environment, as well as to their effect on weather and global climate. Aerosols have been associated with various cardiovascular and pulmonary diseases, and even with increased premature mortality (e.g. Seaton et al., 1995; Utell and Frampton, 2000; Schnelle-Kreis et al., 2009). More than 2 million premature deaths each year can be attributed to the effects of urban air pollution, including particulate matter, ozone ($O_3$), nitrogen dioxide ($NO_2$) and sulphur dioxide ($SO_2$) (WHO, 2005). In addition to local air pollution emissions, aerosol particles that are long-range transported can also have significant health impacts. Liu et al. (2009) estimated that in year 2000 nearly 380 000 premature deaths (for adults age 30 and older) could have been associated to inter-continental transport of $PM_{2.5}$ particles.

Aerosol particles' effects on weather and climate are manifold. They alter the Earth's energy budget directly by scattering and absorbing solar radiation. In lesser extent some aerosols also contribute to scattering, absorption and emission of thermal radiation. Aerosol particles' spatial and vertical distribution as well as their optical properties, underlying surface properties, trace gases and Sun-Earth geometry all together determine whether the direct aerosol radiative effect cools or warms the Earth-atmosphere system. For example, moderately absorbing aerosols might cause cooling over a dark surface, but once transported over a bright surface – such as desert or snow-covered area – the resulting effect can change to warming. Several studies conclude that globally aerosol particles tend to cool the climate under cloud-free conditions, but the estimates of the magnitude vary (e.g. Haywood and Boucher, 2000; Jacobson, 2001; Bellouin et al., 2005; Loeb and Manalo-Smith, 2005; Schulz et al., 2006; Quaas et al., 2008; Bellouin et al., 2008; Garcia et al., 2012; Ma et al., 2014). This is mainly due to the large spatiotemporal variation of the aerosol properties in the

atmosphere, as well as different methods and models used to evaluate the radiative effect. The recent IPCC report (IPCC, 2013) summarizes that the estimates of the global clear-sky direct aerosol radiative effect at the Top-Of-the Atmosphere (TOA) ranges from about $-0.1$ to $-0.8$ $\mathrm{Wm}^{-2}$, observation-based methods giving somewhat more negative estimates than the models. Locally the magnitude of the direct radiative effect can differ considerably from the global mean.

In addition to the direct effect, aerosols affect the climate system and weather indirectly, by changing ice and snow albedos (Hansen and Nazarenko, 2004) or by changing cloud characteristics in various ways (Lohmann and Feichter, 2005). Aerosols can act as cloud condensation or icing nuclei. An increase in the number of aerosol particles results in the increased number of small cloud droplets, which makes clouds appear brighter and reflect solar radiation more efficiently. On the other hand, decrease in the droplet sizes decreases also the precipitation efficiency and thereby prolongs cloud lifetimes. The majority of the cloud-related aerosol indirect effects are estimated to cool the atmosphere (Lohmann and Feichter, 2005; IPCC, 2013), but large uncertainties still exist and the net effect of some indirect processes is still unknown. Aerosol particles can also increase upper tropospheric humidity through deep convection, which in turn has warming effect on climate (Bister and Kulmala, 2011). It has also been shown that already a relatively small amount of black carbon-type absorbing aerosol particles can alter the vertical temperature profile and atmospheric stability, and hence affect the strength of convection (Menon et al., 2002).

From climatic and health perspectives the importance of obtaining information about aerosols' spatial and vertical distribution is evident. While in situ measurements provide accurate information e.g. about aerosol particles' chemical composition, size distribution and local variation, remote sensing measurements have the ability to provide a broader view of the atmospheric aerosol field. The common aspect in different remote sensing instruments is that they use electromagnetic radiation, either from natural sources or emitted by the device itself, to obtain information about atmospheric aerosol particle properties. A remote sensing measurement is an ill-conditioned inversion problem: there are more unknowns than knowns. Hence, assumptions or a priori information e.g. about aerosol particle types are needed to convert the measured radiances into relevant parameters that describe desired aerosol properties.

The most common remote sensing instruments used in aerosol research are sunphotometers, different spaceborne satellite instruments and lidars. Satellite instruments have the capability to globally monitor aerosol particles' spatiotemporal distributions. The majority of the satellite instruments used in aerosol research provide daytime observations over a certain location with temporal coverage that varies from once per day to once per week, depending on the instrument and the orbit. Sunphotometers are ground-based devices that provide

observations at a certain location whenever solar light is available. Both satellite and sun-photometer measurements include observations of column-integrated aerosol extinction, i.e. how much radiation is attenuated due to aerosols in the total atmospheric column. These observations can be carried out only when the sky is cloud-free. Lidars, on the other hand, measure the backscattered signal of the emitted laser pulse. They have the capability to provide vertical distributions of atmospheric aerosol particles, also during night time and under cloudy (but rain-free) conditions. Most of the lidars are ground based, but one lidar is also currently operating onboard a satellite platform.

An example of a visual in situ and remote sensing observation is illustrated in Figure 2, which shows a photo taken on $13^{th}$ Oct. 2008 in Beijing city centre, China, and an image taken by a satellite instrument on the same day. As is seen from the photo, air quality was severely reduced during that day in Beijing due to increased aerosol concentrations. The information from the satellite instrument, on the other hand, reveals the extent of the severe air pollution episode: the haze was not only a local problem over Beijing, but it extended more than 1000 km southward, covering the major part of the densely populated North-Eastern China. In addition to complementing the in situ observations, the advantage of especially spaceborne remote sensing is that they can provide observations over areas or events where carrying out in situ measurements would be impossible. One good example is the eruption of the Eyjafjallajökull volcano in Iceland in 2010, when different satellite instruments provided a wealth of information about the dispersion, height and optical properties of the


Figure 2: An example of a visual in situ (left) and satellite (right) observation on $13^{th}$ Oct. 2008. The photo has been taken in the city centre of Beijing, China, about an hour after the satellite overpass time. The satellite data is a RBG-composite image from the MODerate Imaging Spectroradiometer (MODIS) instrument onboard the Aqua satellite. In the satellite image the bright white areas are clouds while haze due to aerosols appears as different shades of gray.

ash plume (e.g. Toledano et al., 2012; Kahn and Limbacher, 2012; Virtanen et al., 2014). Another important aspect is that remote sensing observations can be used in conjunction with different atmospheric models. Remote sensing observations can be assimilated into different atmospheric models to improve the performance of the model and forecasts (e.g. Collins et al., 2001; Zhang et al., 2008; Sofiev et al., 2009) or they can be used e.g. as a direct input to radiative transfer models to define the radiative effects of aerosols (e.g. Bellouin et al., 2005; Thomas et al., 2013). Remote sensing observations are also used to validate atmospheric or climate models.

The aim of this Thesis is to explore different remote sensing methods to obtain information on aerosol properties and their effect on air quality and climate. Specific objectives of the work presented in this Thesis are:

- To explore the use of a ground-based ceilometer-type lidar to obtain quantitative information on aerosols. The rationale for this study is that ceilometers are designed to observe cloud height, for instance for aviation. At the time of the study they had not been commonly used for monitoring aerosol properties.
- To improve the AATSR dual view retrieval algorithm to provide information on the spatial and temporal variation of aerosols over Eastern China, including the contribution of fine mode aerosol particles.
- To use satellite data to evaluate climate modelling results in a study on climate change over India and China.
- To evaluate the capabilities and limitations of a satellite-based method to estimate the clear-sky shortwave aerosol direct radiative effect.

This introductory part of this Thesis is organized as follows: Sect. 2 introduces briefly the single-scattering and radiative transfer theories that are the basis for aerosol remote sensing. Sect. 3 summarizes the different aerosol remote sensing techniques, and in Sect. 4 the key findings of this Thesis are introduced. The conclusions and future aspects are presented in Sect. 5.

# 2 Basic concepts of atmospheric radiative transfer

Remote sensing instruments that are used to monitor atmospheric constituents measure the intensity, and in some cases also the polarization, of electromagnetic radiation that has propagated within/through the atmosphere, and interacted with the environment. The basic theories behind aerosol remote sensing techniques are those of single-scattering and radiative transfer (multiple scattering) of electromagnetic radiation. In order to extract information about aerosol particles from the measured remote sensing signals, one would need to know

1. how particles' physical properties (composition, size and shape) affect the way that particles interact with the radiation (single-scattering problem), and
2. what interactions radiation has undergone while propagating through the atmosphere before reaching the instrument detector (radiative transfer problem).

However, in the case of aerosol remote sensing the only "known" parameter is the measured signal. To solve this inverse problem, a priori assumptions are needed about particles' physical properties and interactions that the radiation has undergone within the atmosphere. In practice, particles' single-scattering properties need to be solved first, and then those results are used in the radiative transfer problem.

The two major radiative power components of the Earth-atmosphere system are the incoming radiative power from the Sun and the outgoing radiative power from the Earth (Fig. 3). The major part of the incoming solar radiative power falls within the wavelengths of 0.1 $\mu$m and 5.0 $\mu$m, and is typically referred to as shortwave radiation. About half of the radiated power emitted by the Sun is centred between the wavelengths of 0.4 $\mu$m and 0.7 $\mu$m, the light that can be detected by the human eye. The Earth and atmosphere themselves emit radiation that mostly fall at longer, about 4 $\mu$m up to 100 $\mu$m wavelengths. This radiation is not visible to the human eye but is sensed as heat, and therefore referred also as thermal radiation.

Fig. 4 shows a comparison of the solar and the terrestrial emission as well as the wavelength-dependent absorptivity of the atmosphere, which is due to different atmospheric gases. The absorptivity describes the fraction of the radiation that is lost (converted to other forms of energy such as heat) while propagating trough the atmosphere: absorptivity of 0% means that the atmosphere is transparent at these wavebands, while absorptivity of 100% means that all the radiation is "lost" while propagating through the atmosphere.

The electromagnetic spectrum is further divided into a few discrete spectral sub-bands based on their atmospheric characteristics. The ultraviolet (UV) band ranges from 0.1 $\mu$m to approximately 0.4 $\mu$m. Earth's atmosphere is opaque at the major part of the UV spectrum

(Fig. 4), which limits the use of the shortest UV wavebands in the remote sensing applications. UV radiation is the major component in the atmospheric photochemistry, and the longer UV bands are also used for remote sensing of trace gases. The visible band (VIS) extends from approximately 0.4 $\mu$m to 0.7 $\mu$m. The VIS band is an important spectral region from the aerosol remote sensing point of view because at these wavelengths the cloud-free atmosphere is remarkably transparent. This means that the absorption of the radiation at VIS occurs primarily at the surface and not within the atmosphere itself. In addition to aerosol remote sensing, the VIS bands are used to monitor e.g. cloud and surface properties. The near infrared band (NIR) is a continuation for the visible band, and it extends from 0.7 $\mu$m to 4 $\mu$m. The NIR region is characterized by absorption peaks of different gases. At some wavelengths the column integrated absorption is nearly 100%. The NIR wavelengths outside the absorption peaks are also used to monitor aerosols, especially larger particles such as dust, and clouds. The thermal infrared band extends from 4 $\mu$m up to 100 $\mu$m.

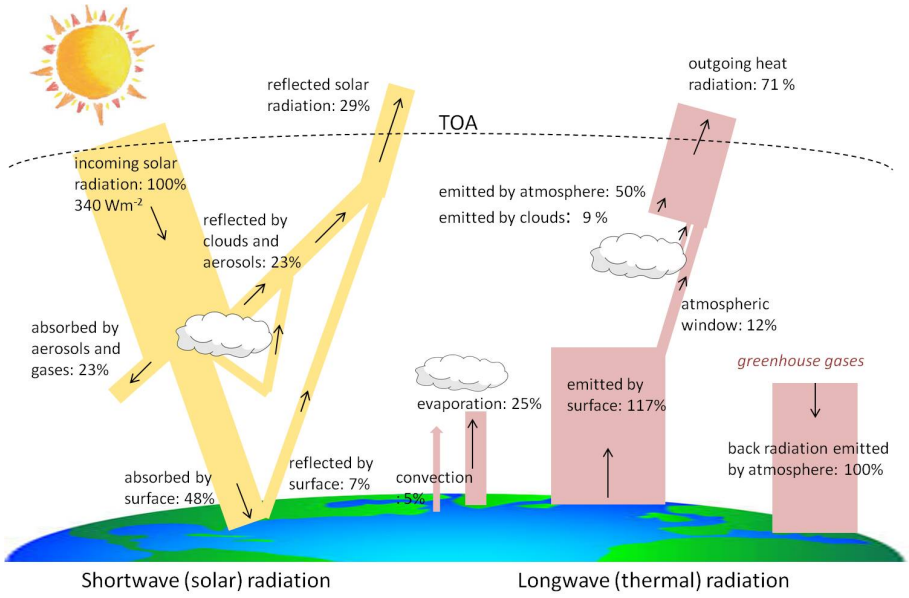


Figure 3: An illustration of the energy balance components of the Earth-atmosphere system. The yellow shapes represent the shortwave (solar) radiation while the red shapes indicate the longwave (thermal) radiation. The figure has been drawn after http://earthobservatory.nasa.gov.

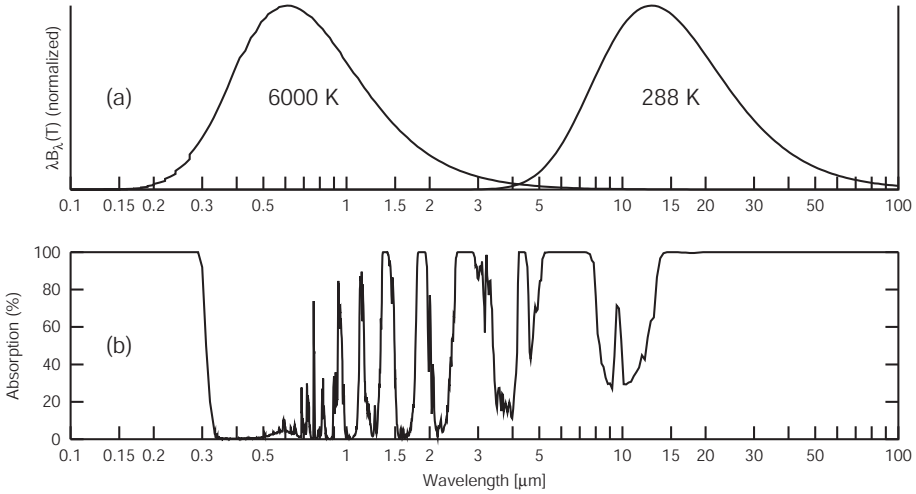


Figure 4: Solar and terrestrial emissions and the absorption properties of the atmosphere. a) represents normalized black-body curves corresponding to the approximate temperature of the Sun's photosphere (6000 K) and a typical terrestrial temperature of 288 K. b) A coarse-resolution depiction of the absorption spectrum of the cloud-free atmosphere. This Figure is adapted from Petty (2006)).

## 2.1 Scattering and absorption

Electromagnetic radiation propagating in the atmosphere undergoes a number of complex processes with the environment. When encountering an object, the electromagnetic radiation can be reflected or reradiated which changes the direction of propagation and/or the radiant energy can be converted into some other form, such as heat or chemical energy. The nature of the interaction between the electromagnetic radiation and an object depends on the wavelength of the radiation, as well as size, shape, and composition of the object. The composition, more precisely the dielectric properties of a particle is described by the complex refractive index $m = n + ik$ where $n$ is related to the phase velocity of the radiation and $ik$ is related to the absorption of the particle.

Scattering is a process where the incident radiation is reradiated into all directions after interacting with a scattering object. The scattering angle $\Theta$ is defined with respect to the direction of propagation of the incident beam (Fig. 5). In the atmosphere scattering occurs when light is interacting with air molecules, aerosol and cloud particles or hydrometeors. The relationship between the size of a particle and the wavelength of the incident radiation is crucial when determining how and how much radiation is scattered, and which method should be used when solving the optical properties, e.g. phase function, scattering and extinction cross sections of a particle (defined later in this section). This relationship can be described with a dimensionless size parameter $x$:

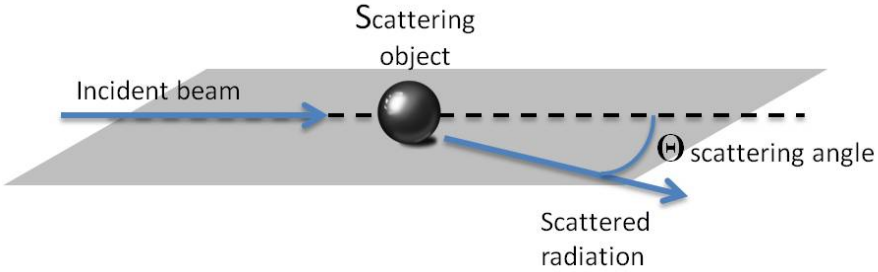


Figure 5: Definition of the scattering angle $\Theta$.

$$x = \frac{D_p \pi}{\lambda} \tag{1}$$

where $D_p$ is the particle diameter and $\lambda$ is the wavelength of the radiation. In most of the atmospheric remote sensing applications that uses the wavelengths from UV to NIR, the most relevant scattering regimes are the Rayleigh (air molecules) and resonance domains (aerosols, cloud droplets) (Fig. 6). The method for solving the single-scattering properties of a particle depends on e.g the size parameter $x$ and the shape of the particle. The optical properties of a spherical and homogeneous particle can be analytically and exactly solved using the Mie theory (Mie, 1908), if particle's refractive index is known. In the Rayleigh regime, where particles are much smaller than the wavelength of incident radiation, the Mie theory reduces to the so called Rayleigh approximation. In the Rayleigh domain the intensity of the scattered radiation varies inversely with the fourth power of the wavelength ($\lambda^{-4}$). The strong wavelength dependence means that shorter wavelengths (blue) of the incoming visible sunlight are scattered more strongly than longer wavelengths (red) in the atmosphere, which is the reason for the blue colour of the sky.

In the resonance domain solving particles' single-scattering properties is more complex than in the Rayleigh regime. If particles are assumed to be homogeneous and spherical (which is not often the case with real aerosol particles), the Mie theory can be used. For non-spherical particles the situation is more complicated, since there is no exact scattering theory for arbitrarily shaped particles. There are some computational methods that can be used to solve the optical properties for irregularly shaped particles, e.g. the T-matrix method (Mishchenko and Travis, 1998) or the Discrete Dipole Approximation (DDA) (Draine and Flatau, 1994).

Properties of radiation can be described by a four-element Stokes vector $S = [I, Q, U, V]^T$. The first element $I$ describes the intensity, which is of interest in the majority of remote sensing applications. The other three elements $(Q, U, V)$ are related to the polarization state,

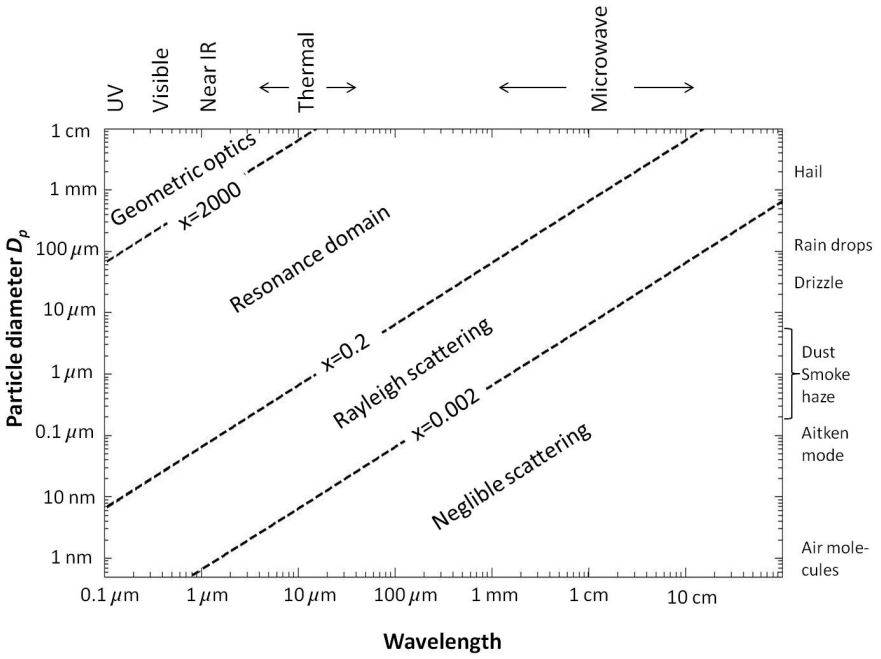


Figure 6: Schematic representation of the different scattering regimes as a function of particle size ($D_p$) and wavelength of the incident radiation. The dashed lines represent different values of the size parameter $x$. This figure is adapted after Petty (2006).

which is used in some of the remote sensing instruments to obtain additional independent information e.g. on particle shape. Sunlight is a mixture of random polarization states, and hence can be considered as unpolarized radiation. In the case of single scattering, i.e. when the radiation is scattered once by a scattering object, a 4x4 phase matrix $\mathbf{P}$ can be used to transform the Stokes vector of incident radiation $S_{inc}$ to the Stokes vector of scattered radiation $S_{sca}$:

$$S_{sca} = \frac{C_{sca}k^2}{4\pi}\mathbf{P}S_{inc} \tag{2}$$

where k is the wavenumber ($2\pi/\lambda$), and $C_{sca}$ is the particle scattering cross section. $C_{sca}$ specifies a hypothetical area that is needed to collect the scattered amount of power from the incident radiation. The scattering efficiency $Q_{sca}$ is the ratio between $C_{sca}$ and the geometrical area of a particle $A$:

$$Q_{sca} = \frac{C_{sca}}{A} \tag{3}$$

The $P_{11}$ element of $\mathbf{P}$ is often referred to as "phase function" that gives the angular distribution of the scattered intensity for incident unpolarized light. $P_{11}(\Theta)$ at $\Theta = 180°$ gives

the scattered intensity in the backscatter direction, whereas forward scattering is given by $P_{11}(0°)$. Fig. 7 illustrates the angular distribution of scattering by showing the Mie-derived $P_{11}(\Theta)$ for four different size parameters $x$. The wavelength in each case is the same (0.5 $\mu$m), but $D_p$ varies from 0.016 $\mu$m ($x$=0.1) to 1.6 $\mu$m ($x$=10). The forward scattering intensifies with increasing $x$ (and in this case also with increasing $D_p$). At the same time as the forward scattering peak intensifies, the rest of the $P_{11}(\Theta)$ becomes more complex as is seen when $x$=10.

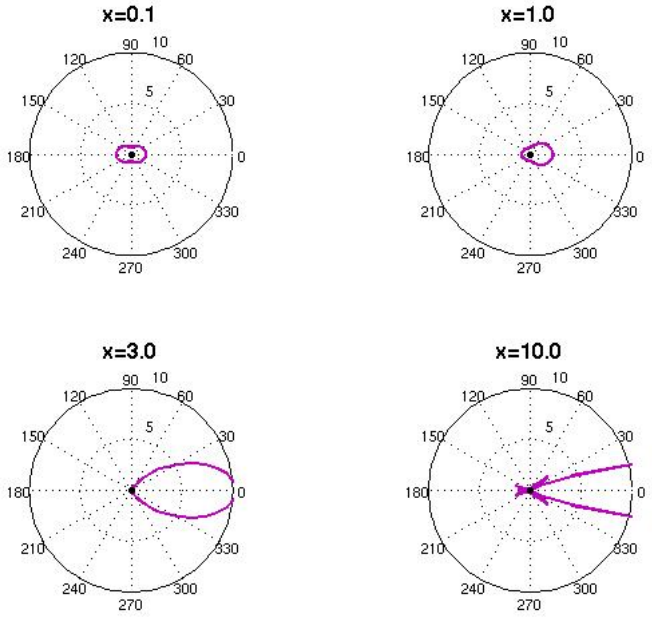


Figure 7: Polar plots of the Mie-derived scattering phase function $P_{11}(\Theta)$ for four different size parameter $x$. In each case the wavelength is 0.5 $\mu$m and refractive index is $m$ =1.45+$i$0.001.

The asymmetry parameter $g$ is defined as

$$g = \frac{1}{2}\int_0^{\pi} P_{11}(\Theta)\cos\Theta\sin\Theta d\Theta \tag{4}$$

Thus, $g$ is an integrated quantity of $P_{11}(\Theta)$ with respect to the scattering angle $\Theta$ (Fig. 5). The values of $g$ range from $-1$ to 1 so that $g < 0$ for particles that scatter more into backward direction ($\Theta > 90°$), and $g > 0$ for particles where forward scattering dominates ($\Theta < 90^o$). For aerosols, $g$ typically ranges between 0.6 and 0.7, whereas for Rayleigh scattering $g = 0$ (e.g. Kokhanovsky and de Leeuw, 2009).

In absorption the incident radiant energy is transformed into particles' internal energy, such

as heat. Particles' ability to absorb light is determined by their composition and indicated by the imaginary part of the refractive index $ik$. The physical meaning of absorption cross section $C_{abs}$ is interpreted similar to $C_{sca}$, and absorption efficiency $Q_{abs}$ is defined analogous to $Q_{sca}$ (Eq. 3):

$$Q_{abs} = \frac{C_{abs}}{A} \tag{5}$$

Similarly, the extinction cross section and extinction efficiency are defined as

$$C_{ext} = C_{sca} + C_{abs} \tag{6}$$

$$Q_{ext} = Q_{sca} + Q_{abs} \tag{7}$$

Thus, extinction describes how much the incident radiation is attenuated due to scattering and absorption. The proportion of scattering in the total extinction is described by the single scattering albedo $\varpi$:

$$\varpi = \frac{C_{sca}}{C_{ext}} \tag{8}$$

For a unit volume containing particles of varying sizes, the extinction coefficient is defined as

$$\sigma_{ext} = \int C_{ext}(D_p) N(D_p) dD_p \tag{9}$$

where $N(D_p)$ is the particle size distribution. The scattering and absorption coefficients $\sigma_{sca}$ and $\sigma_{abs}$ are defined analogously.

The most common aerosol-related parameter that is retrieved from aerosol remote sensing instruments is so called aerosol optical depth (AOD), which is defined as the integral of $\sigma_{ext}$ over the total atmospheric column, from the surface ($z$=0) to the top of the atmosphere ($z$=TOA);

$$AOD(\lambda) = \int_0^{TOA} \sigma_{ext,\lambda}(z) dz \tag{10}$$

Fig. 8 illustrates how AOD correlates with visibility. Since aerosols are most often concentrated in the atmospheric boundary layer, an increase in the AOD typically decreases the

horizontal visibility. Both photos have been taken at the same location in the city centre of Beijing. During the hazy day the AOD at $\lambda$=0.55 $\mu$m was 1.2, which indicates a severe pollution episode. AOD values this high are occasionally observed e.g. over heavily industrialized and populated areas, during dust storms, or in vicinity of forest fires. During the clear day the AOD over Beijing was nearly five times lower (0.25). The global mean AOD obtained from different satellite studies varies between 0.13 and 0.22 (Remer et al., 2008; de Leeuw et al., ress; Holzer-Popp et al., 2013).

The wavelength depencency of AOD is described by the Ångström exponent $AE$ (Ångström, 1929)

$$AE = -\frac{\log \frac{AOD_{\lambda_1}}{AOD_{\lambda_2}}}{\log \frac{\lambda_1}{\lambda_2}} \tag{11}$$

The Ångström exponent can be used as a qualitative indicator of aerosol particle size. For small particles associated with combustion by-products or urban pollution $AE$ values are greater than unity, while for large particles like sea salt and dust $AE$ is less than one (Schuster et al., 2006; Gobbi et al., 2007).

Figure 8: An example of visibility on a hazy and clear day in Beijing. The photos have been taken at the same location in the city centre of Beijing (hazy day 24.10.2009, clear day 26.10.2009). During the hazy day the corresponding AOD at 0.55 $\mu$m was 1.2, whereas during the clear day it was 0.25.

## 2.2 Radiative transfer and direct aerosol radiative effect

The general radiative transfer equation qualitatively sums up the processes that either attenuate or enhance an electromagnetic beam travelling through atmosphere in an arbitrary

direction $ds(s(\vartheta, \phi))$. The radiance $L_\lambda$ of the beam in an arbitrary direction $ds$ is attenuated by absorption and by scattering to other directions, and enhanced by scattering from other directions as well as atmospheric emission. Since in this Thesis the main focus is in the shortwave spectrum ($\lambda < 4$ $\mu$m), the emission term can be neglected (atmospheric emission at these wavelengths is very weak). Accordingly (for shortwave radiation) the radiative transfer equation can be expressed as

$$\frac{dL_\lambda}{ds} = -\sigma_{abs,\lambda}\rho L_\lambda - \sigma_{sca,\lambda}\rho L_\lambda + \frac{\sigma_{sca,\lambda}}{4\pi}\int_0^{2\pi}\int_0^{\pi} P_{11}(\vartheta, \phi, \vartheta'\phi')L_\lambda(\vartheta', \phi')\sin(\vartheta')d\vartheta' d\phi' \quad (12)$$

where $P_{11}(\vartheta, \phi, \vartheta', \phi')$ is the phase function that describes how much radiation from direction $(\vartheta', \phi')$ is scattered into $(\vartheta, \phi)$; $\rho$ is the density of the medium, and $\sigma_{abs,\lambda}\rho$ and $\sigma_{sca,\lambda}\rho$ are the volume absorption and scattering coefficients, respectively. When scattering is involved, to solve Eq. (12) the radiances from all other directions should be known. Hence, solving Eq. (12) by analytical integration is impossible. In the shortwave spectrum where scattering is important, the radiative transfer equation is usually solved using special methods such as "doubling adding" or "discrete ordinates". In climate models more approximate "two stream" methods are usually used because of their less demanding computational burden.

When considering Earth's radiation budget, the parameters of interest are often wavelength integrals of radiances. Rather than considering radiation at some single wavelength $\lambda$, they are often integrated over a wider wavelength band, e.g. over the whole shortwave part of the spectrum. In the integrals over a narrow spectral band the numerous details of gas absorption bands can be accounted accurately. However, when integrating over a wide spectral range, approximate methods are needed to account for the gas absorption to keep the computing times reasonable.

In climate applications the radiation is often described with fluxes $F$. The upward and downward radiative fluxes $F^\downarrow$ and $F^\uparrow$ are defined as integrals of $L$ over the upper or lower hemisphere, respectively;

$$F^\downarrow = \int_0^{2\pi}\int_0^{\pi/2} L(\Theta, \phi)\cos\Theta\sin\Theta d\Theta d\phi \quad (13)$$

$$F^\uparrow = \int_0^{2pi}\int_{\pi/2}^{\pi} L(\Theta, \phi)\cos\Theta\sin\Theta d\Theta d\phi \quad (14)$$

and the net radiative flux $F_{net}$ is defined as

$$F_{net} = F^{\downarrow} - F^{\uparrow}. \tag{15}$$

When considering aerosols and their direct radiative effect on climate, it is often of interest to know how much the aerosols alter the net radiative flux (Fig.3). In this Thesis the focus is on the shortwave part of the electromagnetic spectrum, and hence the aerosol direct radiative effect ($ADRE$) here refers only to the effect at the shortwave part. $ADRE$ is defined as the difference between net fluxes with ($F_{net,aer}$) and without ($F_{net,0}$) aerosol particles present in the atmosphere:

$$ADRE = F_{net,aer} - F_{net,0}. \tag{16}$$

It is noted that $F_{net,0}$ cannot be measured, since aerosol particles are always present in the atmosphere. The value for $F_{net,0}$ is obtained using either a radiative transfer model or approximate methods as in **Paper IV**. $ADRE$ is typically defined separately for clear-sky and all-sky conditions, i.e completely cloud-free skies or all conditions regardless of cloudiness. As in this Thesis $ADRE$ is considered only in the shortwave part of the spectrum, $F^{\downarrow}$ represents the incoming solar radiation at TOA, and it is the same for both aerosol and aerosol-free cases. Hence, at TOA, $ADRE$ can be further reduced to

$$ADRE_{TOA} = F_0^{\uparrow} - F_{aer}^{\uparrow} \tag{17}$$

In the literature the terms "aerosol direct radiative effect" and "forcing" are often mixed and used to refer the total aerosol radiative effect from both natural and anthropogenic aerosols (e.g. Heald et al., 2013). In this Thesis the notation from **Paper IV** is used, where $ADRE$ is considered as a combined radiative effect of anthropogenic and natural aerosols, while the radiative forcing refers to the change in ADRE due to increased level of anthropogenic aerosols compared to the pre-industrial level.The various aerosol indirect radiative effects, e.g. through cloud processes, are out of the scope of this Thesis and hence not considered here. A detailed review of the aerosol indirect radiative effects can be obtained e.g. from Lohmann and Feichter (2005).

# 3 Remote sensing

By definition, remote sensing is a measurement approach for obtaining information about properties of an object without having any direct physical contact with it. The majority

of the different remote sensing techniques used in atmospheric research utilize electromagnetic radiation as a carrier of information about the environment. The instruments measure directional radiant intensity, which generally is not directly the parameter of interest in atmospheric applications. In aerosol remote sensing one of the most common parameters retrieved from the remote sensing measurements is the extinction of light due to aerosols: from satellite measurements it is the column integrated value of aerosol extinction, i.e. the AOD, and from lidars vertically resolved aerosol extinction profile.

Remote sensing is about solving an inverse problem: we have a remote sensing observation but we do not know what is the state and composition of the atmosphere the measured radiation experienced. To solve the inversion problem, a number of direct problems related to particles' single-scattering properties as well as radiative transfer for multiple atmospheric states needs to be solved. To extract the desired information from the measurement, specific inversion algorithms are needed.

Remote sensing techniques can be categorized into two different main classes based on what is the source of the electromagnetic radiation. In passive remote sensing the instruments measure reflected sunlight or thermal radiation emitted from the atmosphere and surface, while in active remote sensing the device itself emits the electromagnetic radiation whose backscattered fraction is then measured. In the following sections different aerosol remote sensing techniques are described. Other remote sensing products not directly related to aerosols but used in this Thesis are described briefly in Sect. 3.4.

## 3.1 Spaceborne passive aerosol remote sensing

Tropospheric aerosols have been monitored with multiple different passive spaceborne instruments for decades. Table 1 summarizes some of the commonly used polar-orbiting instruments. Most of the satellite instruments that are used in aerosol remote sensing are on a Sun synchronous orbit, which means that the satellite's orbital plane has a fixed angle relative to the Sun and it passes over each latitude approximately the same solar time at each orbit. The spatial coverage (swath width) of the instrument defines how often the observations are available over a certain location. Typically the observations are made once per day or in case the swath is narrow, less frequently.

Spaceborne passive remote sensing instruments used in aerosol research measure outgoing solar radiation at the top of the atmosphere. This radiation has undergone complex interactions with the atmosphere and the underlying surface. The quantity measured is the radiance $L_\lambda$ in a certain wavelength band $\Delta\lambda$ ($\lambda$ denotes the center of the wave band), which is the radiant flux per unit solid angle in a given direction [$\mathrm{Wm^{-2}sr^{-1}}$]. In aerosol retrieval

Table 1: A short description of some of the most common passive satellite instruments that are currently used in aerosol research. All of these instruments are on a Sun-synchronous orbit. Typically the sensors are referred by the abbreviations of their official names that are: MODerate Imaging Spectroradiometer (MODIS), Multi-angle Imaging SpectroRadiometer (MISR), Ozone Monitoring Instrument (OMI), Advanced Along-Track Scanning Radiometer (AATSR), POLarization and Directionality of the Earth's Reflectances (POLDER), and Advanced Very High Resolution Radiometer (AVHRR)

| **Sensor** | **MODIS** | **MISR** | **OMI** | **AATSR** | **POLDER** | **AVHRR** |
|---|---|---|---|---|---|---|
| **Platform (Spacecraft)** | Terra Aqua | Terra | Aura | ENVISAT | Myriade series | POES |
| **Swath [km]** | 2330 | 380 | 2600 | 512 | 2400 | 2399 |
| **Resolution at nadir [km]** | 0.25, 0.5, 1.0[1] | 0.275 | 13x24, 13x48[1] | 1.0 | 6x7 | 1.1 |
| **Equatorial overpass** | 10:30, 13:30 | 10:30 | 13:10 | 10:00 | 13:30 | 13:30, 14:30 |
| **In operation (mm/yyyy)** | 12/1999→ 05/2002→ | 12/1999→ | 07/2004→ | 03/2002-04/2012 | 12/2004-10/2013 | 11/1978[2] → |
| **Special features** | onboard two platforms, 36 spectral channels. **(Papers III and IV)** | Nine viewing angles, sensitive to particle shape. | Uses near-UV wavel., information abt. aerosol absorption | Two viewing angles. **(Paper II)** | Measures also polarization, sensitive to particle shape. | Long data record. |

[1] Depends on the spectral channel.

[2] Aerosol data available 01/1988→.

applications a commonly used parameter is normalized $L_\lambda$, or reflectance $\rho$, which is defined as

$$\rho_\lambda = \frac{L_\lambda \cdot \pi}{F_{sun} \cos(\theta_{sun})}. \tag{18}$$

Here $F_{sun}$ is the extraterrestrial solar irradiance and $\theta_{sun}$ is the solar zenith angle. The Sun-satellite measurement geometry is illustrated in Fig 9.

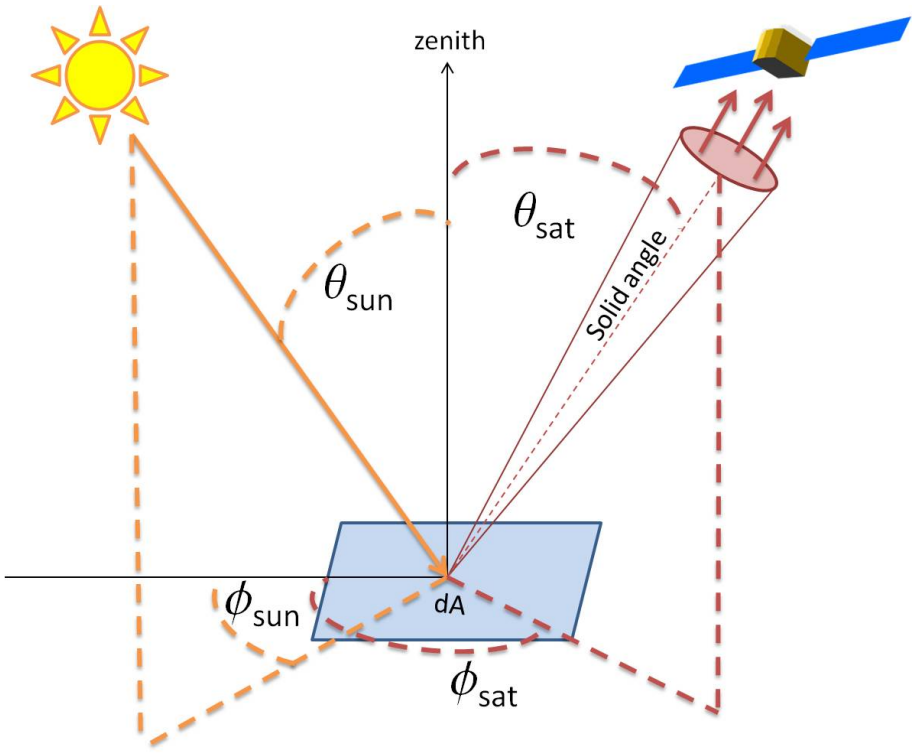


Figure 9: The Sun-satellite measurement geometry.

In the absence of clouds, the measured reflectance has contributions from the atmosphere (air molecules and aerosols), surface, and reflections from outside the sensor's Field-Of-View (FOV). Usually the contribution of reflections from outside the FOV is so small that it can be neglected (e.g. Kokhanovsky and de Leeuw (2009)). Assuming that the plane parallel atmosphere is horizontally homogeneous and that the underlying surface reflects isotropically (Lambertian surface), the reflectance $\rho_\lambda$ at TOA can be expressed essentially as the sum of the atmospheric and the surface contributions:

$$\rho_{\lambda,TOA} = \rho_{\lambda,atm} + \frac{\rho_{\lambda,surf}}{1 - s_\lambda \rho_{\lambda,surf}} T_\lambda, \tag{19}$$

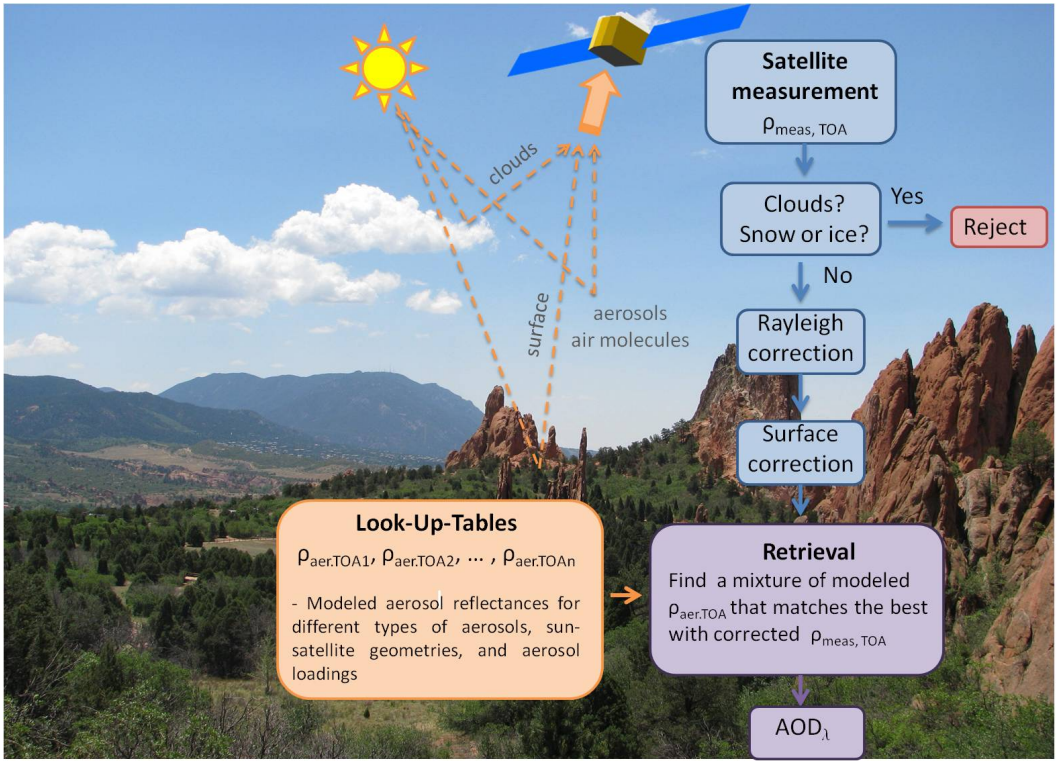


Figure 10: An example structure of a satellite aerosol-retrieval algorithm. This diagram does not apply to any specific instrument but gives a generic outline of a satellite retrieval algorithm.

where $\rho_{\lambda,atm}$ is the atmospheric path reflectance due to scattering and $\rho_{\lambda,surf}$ is the surface reflectance. $T_\lambda$ is the sum of direct and diffuse upward and downward atmospheric transmissions, and $s_\lambda$ is the atmospheric backscattering ratio, i.e. the spherical albedo of the atmosphere. Atmospheric transmission describes the fraction of the initial radiation that remains after propagating through the atmosphere. All the terms in Eq. (19) are dependent on the Sun-satellite geometry.

All aerosol retrieval algorithms share some common elements, outlined in Fig. 10. The purpose of the aerosol retrieval algorithm is essentially to separate the contribution of $\rho_{\lambda,atm}$ from the measured $\rho_{\lambda,TOA}$, and further define the aerosol contribution to $\rho_{\lambda,atm}$. Presently operational aerosol retrieval algorithms do not retrieve aerosol properties over snow/ice or in cloudy conditions, because the signals from these bright targets are much stronger than those from the aerosols. However, recently some progress has been made in attempting to retrieve aerosol optical properties above clouds (Torres et al., 2012; Jethva et al., 2014), and over snow (Mei et al., 2013a,b) using research versions of operational aerosol retrieval algorithms.

Typically the first step in an operational aerosol retrieval algorithm is the identification and

removal of pixels with clouds or snow and ice present. The cloud filtering procedure often includes a number of tests using VIS and NIR channels. Once the cloud-free pixels are found, the surface and Rayleigh (air molecules) corrections are made to the measured $\rho_{\lambda,TOA}$. The performance of the surface correction in the retrieval algorithms vary. Some algorithms (e.g., MODIS; Levy et al., 2013) use an external surface model where the surface properties for different types of vegetation and land cover have been defined. If the instrument has more than one view, an alternative way is to use the observations from multiple views to exclude the surface contribution. In this case additional assumptions about the angular dependence of the surface reflectance and the spectral contribution of aerosols to the measured signal are needed. This is the operating principle of the AATSR ADV algorithm (**Paper II**).

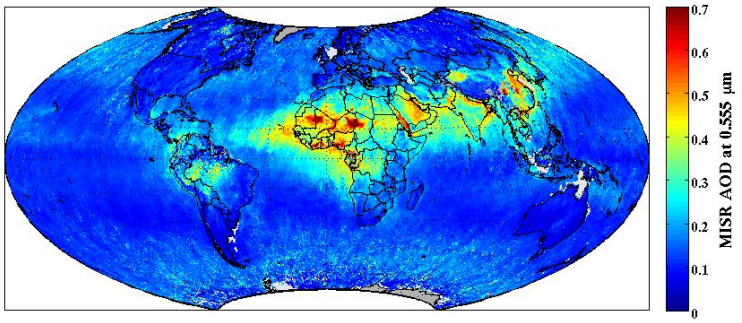


Figure 11: Global distribution of annual mean AOD (year 2010) obtained from the MISR instrument.

To solve the inverse problem and extract the aerosol properties from the surface and Rayleigh-corrected $\rho_{\lambda,TOA}$, a number of direct problems must be solved. Since the aerosol properties in the observed $\rho_{\lambda,atm}$ are not known, the aerosol-related $\rho_{\lambda,atm}$ needs to be modelled for different aerosol types and loadings in the given Sun-satellite geometries. To reduce the computing time that is needed for performing these calculations, pre-calculated matrices i.e. so called Look-Up-Tables (LUTs) are used. Each LUT essentially includes modelled $\rho_{\lambda,atm}$ for a certain aerosol type, at sufficient number of discrete Sun-satellite geometries and discrete aerosol loadings so that all possible atmospheric scenarios are covered. The number of LUTs utilized in an aerosol retrieval varies depending on the algorithm and sensor. Also the method how different aerosol types are mixed varies. In some algorithms LUTs are calculated for fixed mixtures of different aerosol types, whereas in some algorithms each LUT represents a

certain aerosol type and the LUTs are mixed in the retrieval. In the retrieval process itself the measured $\rho_{\lambda,TOA}$ is compared with a mixture of different $\rho_{\lambda,atm}$ from LUTs, and finally the mixture of LUTs that spectrally fits best with the measurements is selected and the corresponding AOD is obtained. Fig. 11 shows as an example the annual mean (year 2010) AOD distribution from the MISR instrument.

## 3.2 Ground-based passive remote sensing of aerosols

Sunphotometry is the simplest form of passive remote sensing (e.g. Kokhanovsky and de Leeuw, 2009). The sunphotometer device itself points at the sun and measures the solar irradiation at certain wave bands attenuated by the atmosphere. It is generally assumed that the sunphotometer measurement is not significantly influenced by the surface, and hence less assumptions are needed than in the satellite remote sensing to derive the aerosol contribution from the measured signal. The aerosol properties can be derived only for cloud-free cases. The sunphotometer signal is given by (Holben et al., 1998)

$$V(\lambda) = V_0(\lambda) d^2 \exp(\tau(\lambda) m) T_g \tag{20}$$

where $V(\lambda)$ is the voltage corresponding to the intensity of the received radiation at wavelength $\lambda$, $V_0(\lambda)$ is the calibration constant, and $d$ is the Earth-Sun distance. The total extinction $\tau(\lambda)$ includes contributions from both aerosols and gases, whereas $T_g$ denotes the transmission of absorbing gases. The optical air mass is defined as $m = (\cos\theta_{sun})^{-1}$.

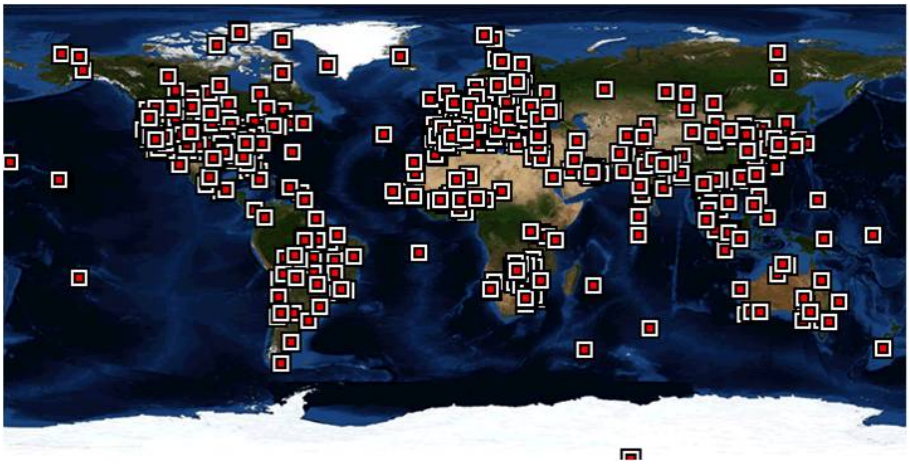

Figure 12: Worldwide locations of the AERONET stations (as of 09/2014). This figure is obtained from http://aeronet.gsfc.nasa.gov/.

AERONET (AErosol RObotic NETwork; http://aeronet.gsfc.nasa.gov; Holben et al. (1998)) is a global ground-based sunphotometer network that monitors aerosol optical, microphysical, and radiative properties (Fig. 12). AERONET uses Sun and sky scanning Cimel sunphotometers that measure spectral sky radiances at known angular distances from the Sun. The primary product of the AERONET network is spectral AOD. In addition to AOD, the AERONET data consist of precipitable water and inversion products such as e.g. single scattering albedo or aerosol size distribution that are extracted from the sunphotometer sky radiance measurements using a special inversion algorithm (Dubovik and King, 2000). All AERONET data are publicly available. AERONET has become the best source of data for validation of the accuracy of satellite aerosol retrievals due to its capability to provide accurate measurements from the ground. In **Paper II** AERONET data from Chinese stations were used to validate the satellite-based AOD, whereas in **Paper IV** AERONET inversion data (spectral $\varpi$) from the same stations were used to get a priori estimate of the aerosol absorption within the study area.

## 3.3 Active remote sensing of aerosols

The key components of an active remote sensing instrument are a transmitter and a receiver. While passive instruments utilize electromagnetic radiation from natural sources, active instruments measure radiation that has been emitted from the device itself. The most commonly known active remote sensing device is a weather radar. Lidar is also a radar-type remote sensing instrument, but it operates at much shorter wavelengths (from 0.250 up to 11.0 $\mu$m) than radars. This makes lidars sensitive to the air molecules and aerosols, in addition to hydrometeors. In contrast to the passive satellite instruments that monitor wide horizontal areas, lidars measure the vertical or slant extinction profiles above/below the instrument. One advantage compared to the passive remote sensing instruments that utilize the solar radiation is that the lidar measurements can be carried out also during the night time. The majority of the lidars are ground based, but Cloud-Aerosol LIdar with Orthogonal Polarization (CALIOP, Winker et al. (2007)) is spaceborne, operating onboard the CALIPSO satellite.

Elastic backscatter lidar is a traditional form of lidar, where the transmitter emits laser pulses at a single wavelength and the detector measures the backscattered signal at the same wavelength. A schematic representation of the lidar measurement geometry is shown in Fig. 14.

The detected lidar signal is described by the lidar equation, which in the case of elastic backscattering can be written as:

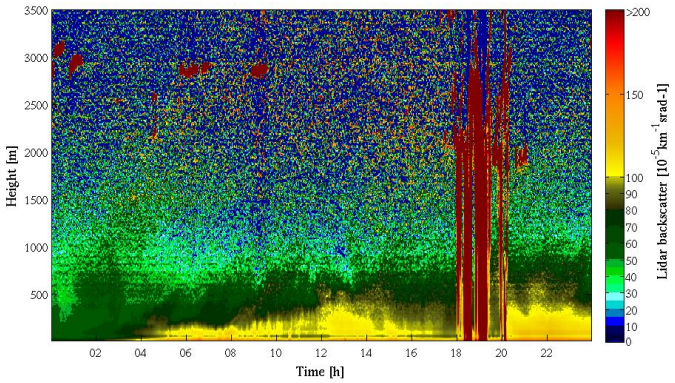


Figure 13: An example of a ceilometer-type lidar (**Paper I**) vertical backscatter profiles at 0.91 $\mu$m wavelength as a function of time. These measurements have been carried out at University of Helsinki Kumpula Campus, Finland. The reddish strong backscattering signals are from clouds, whereas the yellowish and greenish signals are from aerosols. In this case the aerosol signal was unusually strong due to smoke that was transported from forest fires in the Baltic countries to Southern Finland.

$$P(z,\lambda) = K\frac{O(z)}{z^2}\beta(z,\lambda)e^{-2\int_0^z \sigma(z',\lambda)dz'} \tag{21}$$

where $P(z)$ is the received power from a height $z$, and $O(z)$ is the instrument's geometrical overlap function. The exponent is so called two-way transmission term that is related to the extinction of the laser beam. The device-related $K$ is the so called system constant, which is defined as

$$K = P_0\frac{c\tau}{2}A\eta \tag{22}$$

where $P_0$ is the mean power of the emitted laser pulse, $c\tau/2$ is the effective pulse length (Fig. 14), $A$ is the surface area of the primary receiver, and $\eta$ the overall system efficiency. To solve Eq. (21), the ratio between $\beta(z,\lambda)$ and $\sigma(z,\lambda)$ must be known. The most common approach is to assume a linear relationship between the two parameters and define the so called lidar ratio $R$:

$$R = \frac{\sigma(z,\lambda)}{\beta(z,\lambda)} \tag{23}$$

Other possible methods include e.g. the so called Klett method that assumes a power law relation between backscattering and extinction (Klett, 1981). The equations above apply only

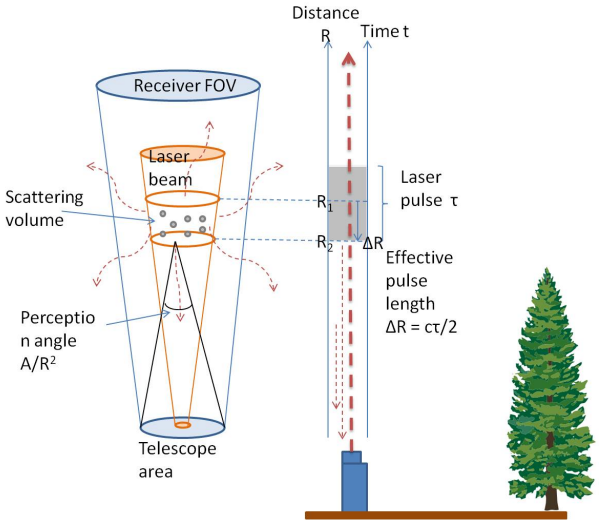


Figure 14: A Schematic representation of a lidar measurement. The right-hand side shows the measurement geometry, whereas the left-hand side is the close up of the contributing measurement volume, defined by the pulse length and the aperture. FOV stands for the Field-Of-View. The figure is drawn after Wadinger (2005).

to elastic backscatter lidars, including the ceilometer-type lidar (Vaisala CL-31) that was used in **Paper I**. The VAISALA CL-31 operates at 0.91 $\mu$m wavelength and is originally designed for monitoring cloud heights. Other more sophisticated research lidars are also widely used in studying different atmospheric constituents. Since some of the research lidars utilize shorter measurement wavelengths, they are more sensitive to aerosol particles and air molecules than the ceilometer-type lidar. Such lidars exploit different measurement techniques and their corresponding lidar equations are typically more complicated. They are also often more demanding to maintain. Differential absorption lidars (DIALs) are used for studying e.g. trace gas or water vapour profiles. They measure the backscattered signal at two different wavelengths so that the other wavelength is coincident with the absorption band of the measured gas. The Doppler lidars, on the other hand, use the Doppler effect from moving objects, often aerosols, to observe e.g. turbulence in the atmosphere. The Raman-lidars utilize inelastic Raman scattering and they are widely used in aerosol research. The European Aerosol Research Lidar Network, EARLINET is a network that is composed of Raman and elastic backscatter lidars operating at 27 stations across Europe (Pappalardo et al., 2014).

## 3.4 Other spaceborne remote sensing parameters

Spaceborne remote sensing instruments are used to provide information about various environmentally important parameters, also other than aerosols. Some of the instruments listed

in Table 1 provide operationally information also about quantities such as the surface albedo (MODIS, AVHRR, MISR) or trace gases (OMI). In **Paper IV**, surface albedo from MODIS was used as an input to a radiative transfer model. The principle of a satellite-based surface retrieval algorithm is also to separate the atmospheric and surface contribution to the measured signal, but in contrast to an aerosol algorithm, now the atmospheric contribution needs to be removed. In addition to the surface albedo, a number of other surface related parameters, such as sea surface temperature or leaf area index are operationally available from multiple satellite instruments.

The Clouds and the Earth's Radiant Energy System (CERES) is an instrument onboard Terra, Aqua and Suomi NPP platforms that retrieves radiant fluxes at the top of the atmosphere. The speciality of the CERES instrument is that it measures the radiances at three broadband channels: shortwave (0.3-5 $\mu$m), infrared window (8-12 $\mu$m), and total (0.3-100$\mu$m) channel. In the CERES retrieval algorithm the measured broadband radiances are converted to TOA-fluxes using angular distribution models (e.g. Loeb and Kato, 2002). The CERES TOA-fluxes include the contribution from the surface, aerosol particles, and air molecules. In **Paper IV** the CERES data was used to derive an observation-based value for the aerosol direct radiative effect over China. The method is described in more detail in Sect. 4.2.1.

# 4 Overview of key results

## 4.1 Air quality applications

The aerosol-related problems in visibility and public health appear foremost in cities and heavily industrialized areas, affecting the lives of hundreds of millions of people. Both **Paper I** and **Paper II** consider aerosol remote sensing in an urban environment from the air quality point of view, but using very different remote sensing methods. **Paper I** uses ground based active remote sensing and the study is carried out in Helsinki, whereas **Paper II** uses passive satellite remote sensing to study aerosol optical depth over Eastern China.

### 4.1.1 Ceilometer-based aerosol measurements

The objective in **Paper I** was to investigate the possibilities to use a simple ceilometer-type lidar (Vaisala CL-31) as a quantitative aerosol measurement instrument. The advantages of a ceilometer-type lidar is that it is relatively easy to maintain, eye-safe, and less costly when compared to the more sophisticated research lidars. Also, the lowest detection range for Vaisala CL-31 ceilometer is about 30 m above the device, which is considerably less than for most of the other types of lidars. Ceilometers that are originally designed for observing cloud heights, have been used for years e.g. in major airports all over the world, and thus potentially offer an extensive, readily available measurement network. The ceilometer used in **Paper I** was situated at the University of Helsinki, Kumpula Campus. Close to the lidar were located the SMEAR III station (Järvi et al., 2009) that provided supporting in situ data on aerosol particles. Helsinki is one of the cleanest metropolitan areas in Europe in terms of air quality (YTV, 2007). Overall the air quality is considered good or satisfactory, but it can temporarily decrease especially in the vicinity of the busy roads or during some episodic event e.g. in the spring, when the streets are cleaned from the sand after winter and atmospheric conditions are stable and preventing vertical mixing.

The Vaisala CL-31 ceilometer used in the study reports the backscattered signal with 10 m vertical resolution. To study whether quantitative information about aerosols could be extracted from the lidar signal, the measured backscattering from a constant height (30 m) was compared with modelled backscattering. The backscattered signal was modelled using measured size distributions of dry aerosols from the SMEAR III station. Since information about aerosol particles' composition and shape was not available, the backscattered signal was modelled using different assumptions about the refractive index and shape. The refractive indices and shapes were selected to represent the boundaries within which the real shapes and composition of aerosol particles were assumed to vary. Results showed a marked difference

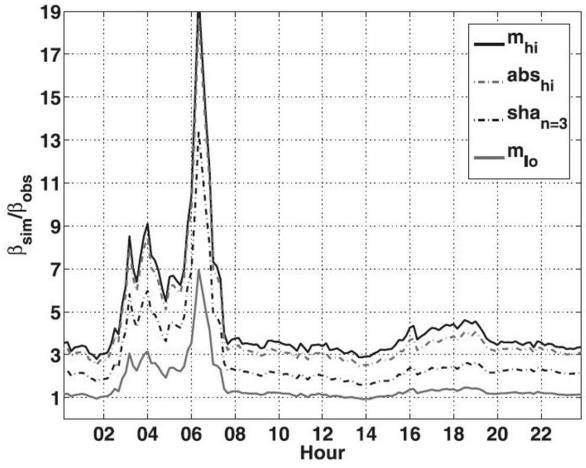


Figure 15: Comparison of measured ($\beta_{obs}$) and theoretically calculated ($\beta_{sim}$) backscattering coefficient $\beta$ represented as a ratio of modelled-to-observed $\beta$ (adapted from **Paper I**). Results are shown for the following cases: spherical particles with refractive indexes $m = 1.5 + 0i$ ($m_{hi}$), $m = 1.3 + 0i$ ($m_{lo}$), and $m = 1.5 + 0.005i$ ($abs_{hi}$), and non-spherical particles with $m = 1.5 + 0i$ (spheroids, $sha_{n=3}$).

between the measurements and the simulated backscattering, which was, however, nearly constant over time (Fig. 15). This indicated that the ceilometer could potentially provide quantitative information about aerosols. Some of the systematic difference could be explained by the parameters assumed for the computations and/or the instrument calibration. As Fig. 15 shows, occasionally large differences between modelled and observed values were also observed, when the modelled backscattering could be over 10 times higher than the observed one. This was most likely related to the differences in the measurement volumes at the lidar measurement height and at the size distribution measurement site. The in situ measurement site was located several hundreds of meters away and more than 40 m below the ceilometer measurement. The increase in aerosol concentration at the size distribution measurement site, and hence very high simulated backscattering were most likely related to some local aerosol source (ongoing construction work near the size distribution measurements) or unfavourable meteorological conditions (weak vertical mixing). Overall the results from this study showed that in some applications the ceilometer-type lidar have sufficient accuracy for quantitative aerosol measurements.

### 4.1.2 AOD retrievals over China

Air pollution is one of the biggest environmental health risks in Asia. With strongly growing population and economies, the increase in anthropogenic emissions is evident. In **Paper**

**II** AATSR retrievals of aerosol optical properties over Eastern China were presented. The AATSR instrument operated onboard the ENVISAT platform (until 04/2012), and it provided observations about every third day at about 10 a.m. local time. In this work the study area covered the most densely populated part of Eastern China, where air quality is often very bad due to extremely high anthropogenic emissions. This was the first study where an improved version of the AATSR dual-view (ADV) algorithm was used, after it had been transferred from the Netherlands Organisation for Applied Scientific Research (TNO) to the Finnish Meteorological Institute and the University of Helsinki, and had been further developed in Finland. Since the time of this study the development of the ADV algorithm has continued in Finland, and the retrievals have been extended to the global scale. The objective in this study was, first, to find the proper aerosol models for the ADV-algorithm that would describe the aerosol mixture within the study area, and second, to retrieve aerosol properties over the study area for year 2008, which was of special interest due to the summer Olympic Games hosted in Beijing in August.

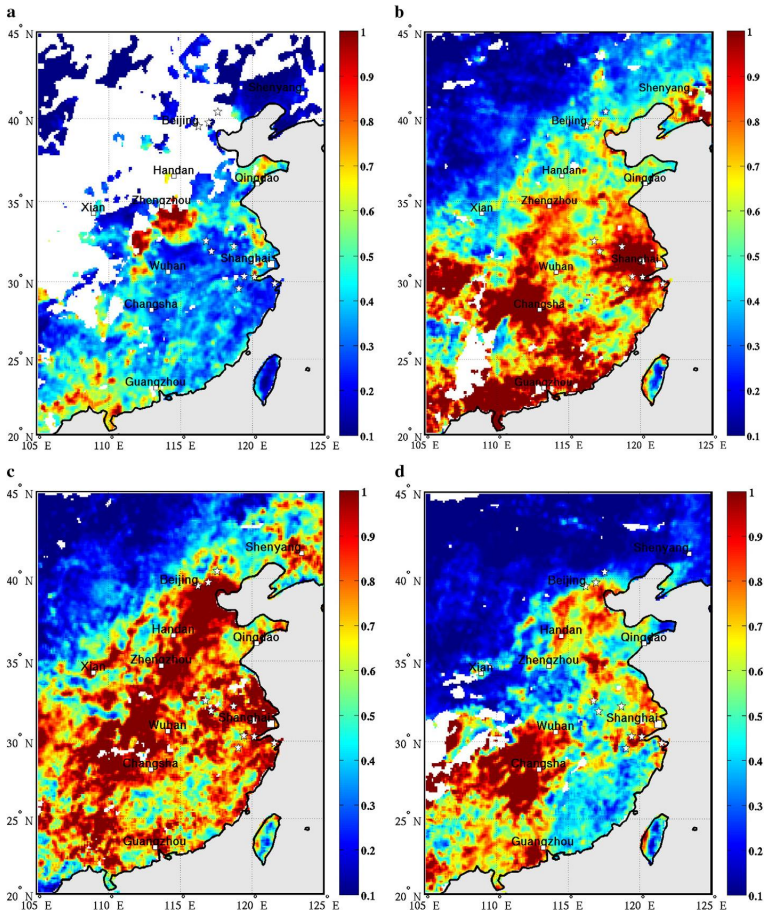


Figure 16: Seasonal averages of AODs over Eastern China for 2008 retrieved with the AATSR ADV-algorithm (adapted from **Paper II**).

The ADV algorithm is designed to retrieve aerosol properties over land, including AOD at 0.555 and 0.659 $\mu$m wavelength, and the mixing ratio for the fine mode particles (i.e. fine mode particle contribution to the total AOD; in this context for fine mode particles $D_p < 1.0$ $\mu$m). The special feature in the ADV algorithm is that it exploits the AATSR instrument's two measurement angles, nadir and 55° forward at 1.6 $\mu$m wavelength, to define the surface contribution from the measured reflectance, and thus makes the use of an additional surface model unnecessary in the retrieval. The version of the ADV algorithm that was used in **Paper II** included one fine and one coarse mode aerosol model (as a LUT) that were mixed in the retrieval process to find the best match with the measured AATSR reflectance. Before the actual retrievals, various combinations of five different LUTs (three for fine mode and two for coarse mode particles) were tested in the ADV-algorithm to find the aerosol models that describe best the aerosol particles within the study area. The decision of the two aerosol models to be used in the ADV-retrieval was made by comparing the retrieved AODs against AERONET observations. The ADV retrievals showed that in the majority of the cases at least 90% of the total AOD originated from the fine mode particles, and hence the selection of a proper fine mode model was especially important. The differences between the different combinations of aerosol models were minor when AOD<0.5, but were more pronounced when AOD>0.5. The best agreement with AERONET observations was obtained with a combination of a fine mode "industrial pollution"-type aerosol model ($m = 1.41 + i0.006$) and a coarse mode "neutral"-type aerosol model ($m = 1.43 + i0.008$). The chosen refractive indices appeared optimal for the retrieval, because increasing or decreasing the fine mode particle absorption decreased the agreement with the AERONET observations, especially when AOD>0.5. The selected aerosol models were used to retrieve the AOD for 2008 over the whole study area.

The AATSR retrievals show a seasonal variation of the AODs (Fig. 16) and mixing ratios over the areas with strong anthropogenic activity; whereas, over rural areas the AODs and mixing ratios were low throughout the year. Despite the seasonal variation, the contribution of fine mode particles to the total AOD remained over 70% throughout the year over densely populated and industrialized areas. Over the largest cities and industrial centres the total AOD tended to have slightly higher fine-mode-particle contributions than in the surrounding areas except during winter time, when the fine-mode-particle contribution was elevated throughout the study area. The results indicated that the air quality decreased especially during the summer, when AOD values as high as 1.0 were observed over the whole eastern part of China. The combination of high humidity and high concentrations of gaseous pollutants, dust, and high temperatures in stagnant air were favourable conditions for the formation of smog and thus increased AOD. During the summer, the AERONET observations also showed few smog episodes with AODs exceeding 3.0 (at 0.55 $\mu$m) in the Beijing and Shanghai areas. For those days there were no ENVISAT overpasses over those locations.

## 4.2 Satellite remote sensing in climate-related studies

**Papers III** and **IV** introduce two different aspects of how the satellite data can be utilized in climate studies. Both studies concentrate on Asia (China and India), which is an important region from the climate point of view due to its high particulate emissions. In **Paper III** the performance of a climate-aerosol model (ECHAM5-HAM) was evaluated by comparing the simulated AODs to satellite observations (in this case MODIS coll. 5 AOD). Results showed that the model reproduced observed seasonal AOD variation over India adequately, but the model values were systematically lower than those measured by MODIS. In China the model also showed similar seasonal variations, but again underestimated the AOD during winter and spring. The agreement between observed and modelled AODs was better during the latter half of the year. The largest model underestimations were observed in India and China during seasons when the contribution of dust to AOD is largest, which implies a possible problem in the dust source estimation in ECHAM5-HAM. **Paper IV** introduces another way to use satellite data in climate studies. In the following subsection a more detailed description of the method and results for deriving satellite-based estimates for $ADRE$ are given.

### 4.2.1 Observation-based estimates of aerosol direct radiative effect

During the past decade, an increasing number of observation-based studies of the shortwave aerosol direct radiative effect $ADRE$ have been carried out, where remote sensing from space plays an important role. In the majority of the studies, the satellite observations, most often AODs, are used as input to radiative transfer codes to define the TOA fluxes needed to derive $ADRE$. Another but less utilized remote sensing-based approach is to use coincident AOD observations e.g. from MODIS and broadband flux observations from CERES to estimate $ADRE$. The advantage of this approach is that the outgoing shortwave flux with aerosols at TOA is directly obtained from CERES measurements, so there is no need to use models to estimate the aerosol properties to infer $ADRE$ (Loeb and Manalo-Smith, 2005). Further, the instantaneous aerosol-free flux at TOA ($F_0^{\uparrow}$) is estimated using linear regression between coincident AOD and TOA flux observations, and hence additional information about surface albedo and radiative transfer simulations are not needed. Even though this method has been used in a number of publications (e.g. Loeb and Manalo-Smith, 2005; Zhao et al., 2008; Christopher, 2011; Patadia et al., 2008; Sena et al., 2013), less focus has been paid to the method itself and to a careful examination of the various assumptions included in this approach. In this work the main goals were to study the method in more detail as well as its applicability over Eastern China, and to derive a satellite-based estimate of $ADRE$ over the study area.

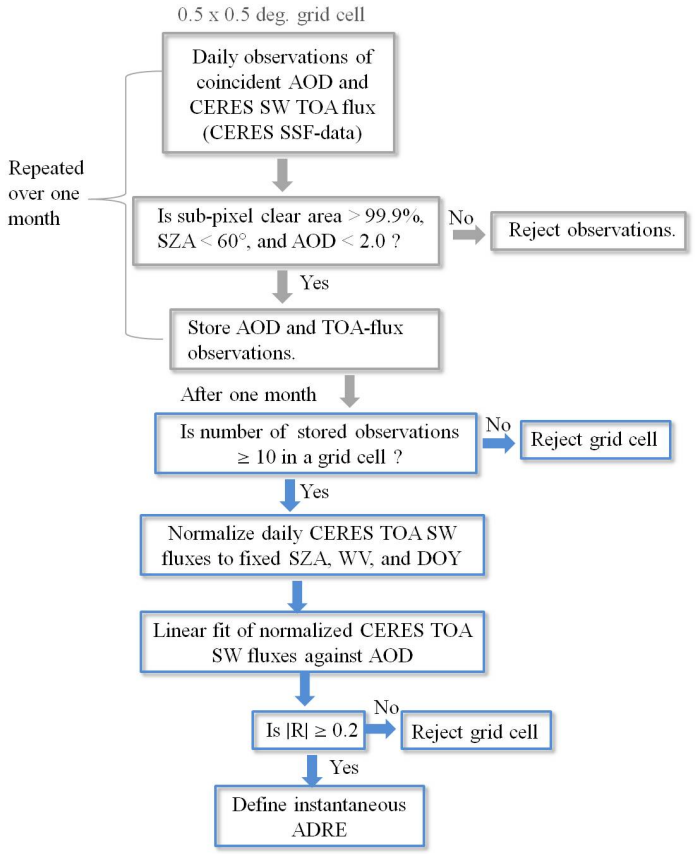


Figure 17: A schematic representation of the different steps needed to determine *ADRE* from the coincident MODIS AOD and CERES SW TOA flux observations (adapted from **Paper IV**).

Deriving an estimate for the aerosol-free TOA flux plays a key role in this satellite-based approach. Fig 17 illustrates the different steps needed to define *ADRE* from the coincident AOD and TOA flux observations. An estimate for the aerosol-free flux $F_0^{\uparrow}$ is obtained by collecting daily observations of coincident TOA-fluxes and AODs over one month in each 0.5x0.5° grid cell. By assuming that the changes in the TOA fluxes are mainly related to changes in aerosol loading, and not to changes in e.g. the effective aerosol type, a linear relationship between CERES TOA SW-fluxes and MODIS AODs can be established in each grid cell. The resulting regression line is interpolated to AOD=0, and the corresponding flux value is the monthly mean value for the aerosol-free flux $F_0^{\uparrow}$. However, in this study it was shown that during one month when the observations are collected, changes in solar zenith angle, water vapour, and Earth-Sun distance created noise in the observed CERES TOA fluxes. This affects the linear regression between AODs and TOA fluxes, and eventually to the estimated value of the aerosol-free TOA flux. To reduce the variation not related to aerosols, a normalization procedure to a fixed solar zenith angle, water vapour content,

and day-of-year was applied to the observed CERES fluxes before the actual linear fit. The reference fluxes were modelled with a radiative transfer code. The results showed that normalization procedure decreased the noise in the observed CERES TOA fluxes and improved the correlation between the observed TOA fluxes and AODs considerably (Fig. 18).

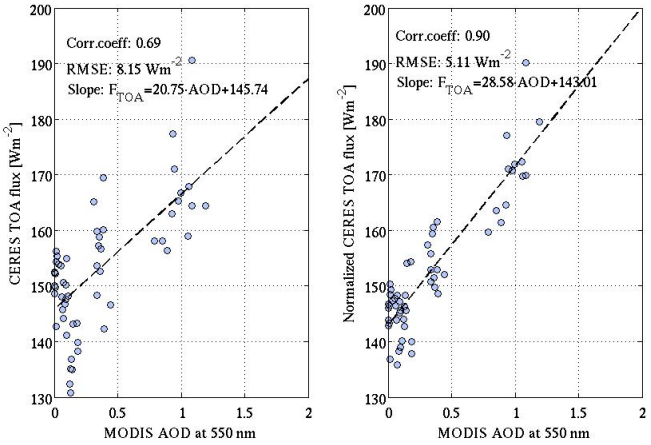


Figure 18: An example of the determination of $F_0^{\uparrow}$ in one grid cell for one month without (left) and with (right) the normalization procedure (adapted from **Paper IV**).

The goodness of the satellite-based *ADRE* estimate is to a large extent dictated by how good the estimate for the aerosol-free TOA flux is. In this study it was shown that the satellite-based method is capable of producing qualitatively similar aerosol-free TOA flux pattern to what is obtained with a radiative transfer model, but locally the absolute values might differ. Overall, in 58% of the cases, the satellite-based $F_0^{\uparrow}$ was within 10 $\mathrm{Wm}^{-2}$ (about 5-7% difference) from the modelled value. Results show that the difference between satellite-based and modelled $F_0^{\uparrow}$ was smaller for grid cells where the correlation between CERES fluxes and MODIS AODs was high (R>0.6).

The *ADRE* was derived over Eastern China for March-October 2009, after the normalization procedure to all observed CERES fluxes was applied and the satellite-based aerosol-free TOA fluxes had been defined. The *ADRE* that is derived from the satellite observations is the instantaneous value, i.e. it represents *ADRE* at the time of the satellite overpass (about 10:30 local time). To be able to compare the results with other *ADRE* studies, the instantaneous values were temporally integrated into 24h $ADRE_{24h}$ using a radiative transfer model. In the integration only solar zenith angle variation was accounted for.

Results showed that the satellite-based ADRE indicated cooling over the major part of the study area (Fig. 19). The diurnally averaged median clear-sky $ADRE_{24h}$ over the study area was -5.1 $\mathrm{Wm}^{-2}$, which is in line with the values reported in the literature (e.g. Thomas

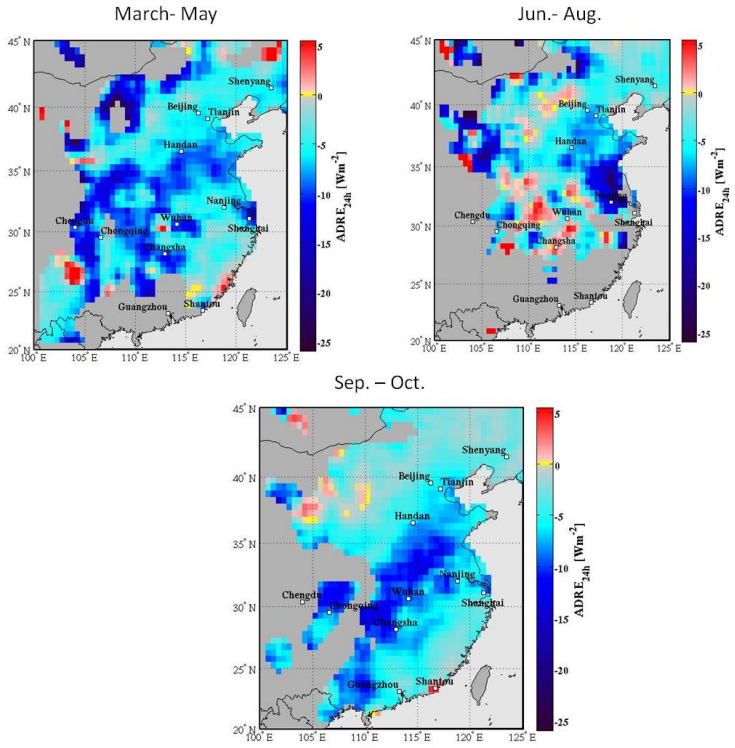


Figure 19: The seasonal medians of diurnally averaged $ADRE_{24}$ over Eastern China (Mar.-Oct. 2009) obtained using the satellite-based method (adapted from **Paper IV**).

et al., 2013). Over heavily industrialized areas with high aerosol concentrations (AOD>0.5) the cooling at TOA was two to over three times stronger than the median $ADRE_{24h}$ over the whole area. Locally some positive $ADRE_{24}$s, i.e. warming at TOA, were observed, especially during the summer months. In some of the cases the warming effect was most probably a method artefact related to some systematic change of aerosol type, sub-visual cloud contamination, or both.

# 5 Conclusions and future aspects

In this Thesis the applicability of various remote sensing data for air quality and climate studies has been shown. In some applications ceilometers have the required accuracy to be used as an quantitative aerosol measurement instrument. Potentially an extensive, readily available measurement network could also be available since the ceilometers are originally designed for observing cloud heights, and thus they have been used for years e.g. in major airports all over the world. Satellite observations, on the other hand, can provide a wide horizontal view on the aerosol field. The first study, where an improved version of the AATSR satellite algorithm was used, showed that AOD can be retrieved with sufficient accuracy over Eastern China. In addition, the AATSR algorithm can provide valuable information about the fine mode particle contribution to the total AOD. These satellite observations could also be used in a variety of applications, e.g. in estimating particulate emissions and tracking pollutant plumes or as a supporting data in air quality studies.

Currently the satellite-based AOD is available from some instruments for a time period of over 10 years. This data can be used to evaluate global changes in aerosol loadings and, on the other hand, compare the results with climate models. However, attention should be paid on how climate models and satellite observations are compared, since satellite observations are "snapshots" of the aerosol field, which are strictly speaking representative only of the time of the satellite overpass. A meaningful way to compare satellite and model data would be to sample only those model values when satellite data were available.

In this Thesis also a satellite-based method for estimating the clear-sky shortwave aerosol direct radiative effect ADRE (at the top of the atmosphere) is investigated. The method uses coincident observations from two different satellite instruments to define ADRE. The value of this study is that it provides an observation-based estimate of a quantity that is most often estimated using models. In fact, applying the satellite-based method over Eastern China showed that, overall, the satellite-based estimates of ADRE are in agreement with model-based estimates reported in the literature.

In the future air quality studies could benefit more from the synergy of vertically resolving lidar-type and horizontally extensive satellite-type remote sensing observations (Fig. 20). By combining the vertical and horizontal information, a three-dimensional view of the aerosol field could be obtained. In addition, in cloudy cases lidar-type remote sensing measurements could provide information about aerosols when operational satellite observations are not available. Recently, a new network in Finland has been established that consists of five different sites, where a Doppler lidar and a ceilometer operate side-by-side providing near-real time information on air pollution and boundary layer properties (Hirsikko et al., 2014). Hence, in the future, more detailed information about air quality episodes can be obtained

in Finland, especially if the synergy with the satellites is also capitalized. Another recent example of the synergy of remote sensing devices is the Generalized Aerosol Retrieval from Radiometer and LIdar Combined data (GARRLIC) retrieval algorithm, that uses both lidar and sunphotometer observations (Lopatin et al., 2013). Such synergetic retrievals allow the retrieval of parameters that have not been available from remote sensing instruments before, e.g. the vertical distribution of single scattering albedo.

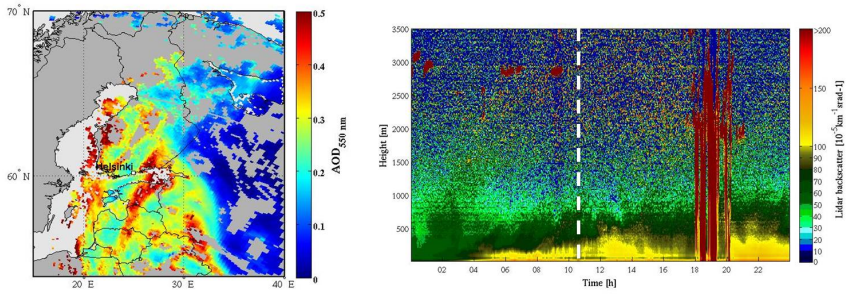


Figure 20: An example of the synergy of two different remote sensing devices for observing forest fire smoke plumes. The left panel shows the horizontal distribution of AOD from MODIS Terra on 25.8.2005 while the right panel shows the ceilometer vertical backscattering profiles measured at Helsinki Kumpula Campus on the same day. The white dashed line indicates the time of the satellite overpass.

In addition to the most common parameters (e.g. AOD) that are provided operationally by multiple remote sensing instruments, satellite observations can be used in new ways to study phenomena that are not directly observable by remote sensing methods. One example is shown in **Paper IV**, and another example is a recent work by Sundström et al. (2014), where information about nucleation mode particles are obtained by combining satellite based data about AOD, trace gases and UV-radiation, i.e. the components that affect new particle formation. Utilizing and combining different parameters not only from the satellite data, but also from other remote sensing instruments will provide new views and applications on both air quality and climate studies in the future.

# 6 Summary of papers and the author's contribution

**Paper I** investigates whether a commercial ceilometer-type lidar can be used as a quantitative aerosol measurement instrument. To assess this, the ceilometer signal at a constant height close to the surface was compared with modelled backscattering based on in situ measured dry-particle size distribution. The results show that the difference between simulated and measured backscattering was mainly constant, and within the uncertainties involved. Overall the results from this study show that in some applications the ceilometer-type lidar might have sufficient accuracy for quantitative aerosol measurements. My responsibilities in this study were to analyse the ceilometer data and calculate the theoretical backscattering using the dry-particle size distributions provided by Dr. Tuukka Petäjä and the aerosol optical properties provided by Dr. Timo Nousiainen. I was also responsible for analysing the results and writing most of the paper.

**Paper II** presents AOD retrievals over Eastern China with the AATSR Dual View (ADV) algorithm. First, several aerosol models were tested in the ADV algorithm to identify the models that describe best the aerosol properties within the study area. The best agreement with AERONET AOD was obtained with "industrial pollution" as a fine-mode model and "neutral" as the coarse-mode model. These models were then utilized in the ADV algorithm to retrieve the AODs and the mixing ratios (contribution of fine mode aerosols to the total AOD) over Eastern China for 2008. The results show that the fine mode particles contributed more than 70% of the total AOD over areas with high anthropogenic activity. Air quality was decreased especially during summer, when also meteorological conditions were favourable for smog formation. I had the main responsibility to carry out this study. I created the aerosol models used in the ADV algorithm as well as ran all the ADV retrievals and executed the comparisons with the AERONET data. I also analysed the results, and wrote most of the paper.

**Paper III** employs a climate-aerosol model (ECHAM5-HAM) to study the spatial and temporal variability of aerosol properties over India and China for recent (year 2006) and future conditions (year 2020). The modelled aerosol species were sulphate, black carbon, organic carbon, mineral dust and sea salt. Results show that the Indian and Chinese aerosol characteristics and seasonal cycles differ from each other. India had higher concentrations of black and organic carbon, while in China the sulphate concentration was higher. The model-based seasonal cycles for present day AOD in India and China were similar to those obtained from the MODIS satellite data. In this study my responsibilities were to provide the MODIS coll. 5 AOD for a comparison with the model results. I analysed the satellite data, plotted satellite based annual AOD averages over India and China (Figures 6 and 7 in **Paper III**), and wrote part of the satellite related text.

**Paper IV** investigates a satellite-based method for determining the direct aerosol radiative effect ($ADRE$) over Eastern China. The method uses coincident observations of the SW TOA fluxes from CERES and AODs from MODIS to estimate the aerosol-free TOA flux needed to determine the $ADRE$. The study focuses on studying the method itself, and its application to derive $ADRE$ over Eastern China. A new normalization procedure of the observed CERES fluxes to a fixed solar zenith angle, water vapour content, and day-of-year was introduced, which reduced the noise in the observations due to non-aerosol factors. After the normalization, the values of aerosol-free fluxes were defined from the linear fitting between normalized CERES fluxes and MODIS AODs. Results show that $ADRE$ is mostly negative over the study area. Locally the variation from the median $ADRE$ is large, and strongest cooling is observed over the most polluted areas. In some cases $ADRE$ is locally also positive, but those are most likely method artefacts related to some systematic change in aerosol type, sub-visual clouds, or both. I had the main responsibility to carry out the study. I collected the satellite data, carried out the radiative transfer simulations, and created scripts to calculate the satellite-based $ADRE$. I also analysed the results and was responsible for writing the paper.

# References


Ångström, A. (1929). On the atmospherc transmission of Sun radiation and on dust in the air. *Geogr. Ann.*, 11:156–166.

Bellouin, N., Boucher, O., Haywood, J., and Reddy, M. (2005). Global estimate of aerosol direct radiative forcing from satellite measurements. *Nature*, 438:1138–1141.

Bellouin, N., Jones, A., Haywood, J., and Christopher, S. (2008). Updated estimate of aerosol direct radiative forcing from satellite observations and comparison against the Hadley Centre climate model. *J. Geophys. Res.*, 113(D10205).

Bister, M. and Kulmala, M. (2011). Anthropogenic aerosols may have increased upper tropospheric humidity in the 20th century. *Atmos. Chem. Phys.*, 11(9):4577–4586.

Christopher, S. A. (2011). Satellite remote sensing methods for estimating clear sky shortwave Top of atmosphere fluxes used for aerosol studies over the global oceans. *Remote Sens. Environ.*, 115:3002–3006.

Collins, W., Rasch, P., Eaton, B., Khattatov, B., Lamarque, J.-F., and Zender, C. (2001). Simulating aerosols using a chemical transport model with assimilation of satellite aerosol retrievals: Methodology for INDOEX. *J. Geophys. Res.*, 106(D7):7313–7336.

Dal Maso, M., Kulmala, M., Riipinen, I., and W (2005). Formation and growth of fresh atmospheric aerosols: eight years of aerosol size distribution data from SMEAR II, hyytil, finland. *Boreal Env. Res.*, 10:323–336.

de Leeuw, G., Holzer-Popp, T., Bevane, S., Daviese, W., Descloitres, J., Graingerg, R., Griesfellerh, J., Heckel, A., Kinne, S., , Klüser, L., Kolmonen, P., Litvinov, P., Martynenko, D., North, P., Ovigneur, B., Pascal, N., Poulsen, C., Ramon, D., Schulz, M., Siddans, R., Sogacheva, L., Tanre, D., Thomas, G., Virtanen, T., von Hoyningen-Hüne, W., Vountas, M., and Pinnock, S. (2013, in press). Evaluation of seven European aerosol optical depth retrieval algorithms for climate analysis. *Remote Sens. Environ.*

Draine, B. T. and Flatau, P. J. (1994). Discrete-dipole approximation for scattering calculations. *J. Opt. Soc. Amer*, 11:1491–1499.

Dubovik, O. and King, M. (2000). A flexible inversion algorithm for retrieval of aerosol optical properties from Sun and sky radiance measurements,. *J. Geophys. Res.*, 105(D16):20673–20696.

Garcia, O., Diaz, J., Exposito, F., Diaz, A., Dubovik, O., Derimian, Y., Dubuisson, P., and J.-C., R. (2012). Shortwave radiative forcing and efficiency of key aerosol types using AERONET data. *Atmos. Chem. Phys.*, 12:5129–5145.

Gobbi, G. P., Kaufman, Y. J., Koren, I., and Eck, T. F. (2007). Classification of aerosol properties derived from AERONET direct sun data. *Atmos. Chem. Phys.*, 7(2):453–458.

Hansen, J. and Nazarenko, L. (2004). Soot climate forcing via snow and ice albedos. *Proc. Natl. Acad. Sci. USA*, 101(2):423–428.

Haywood, J. and Boucher, O. (2000). Estimated of the direct and indirect radiative forcing due to Tropospheric aerosols: A review. *Rev. Geophys.*, 38(4):513–543.

Heald, C. L., Ridley, D. A., Kroll, J. H., Barrett, S. R. H., Cady-Pereira, K. E., Alvarado, M. J., and Holmes, C. D. (2013). Beyond direct radiative forcing: the case for characterizing the direct radiative effect of aerosols. *Atmos. Chem. Phys. Discuss.*, 13(12):32925–32961.

Hirsikko, A., O'Connor, E. J., Komppula, M., Korhonen, K., Pfüller, A., Giannakaki, E., Wood, C. R., Bauer-Pfundstein, M., Poikonen, A., Karppinen, T., Lonka, H., Kurri, M., Heinonen, J., Moisseev, D., Asmi, E., Aaltonen, V., Nordbo, A., Rodriguez, E., Lihavainen, H., Laaksonen, A., Lehtinen, K. E. J., Laurila, T., Petäjä, T., Kulmala, M., and Viisanen, Y. (2014). Observing wind, aerosol particles, cloud and precipitation: Finland's new ground-based remote-sensing network. *Atmos. Meas. Tech.*, 7(5):1351–1375.

Holben, B., Eck, T. F., Slutsker, I., Tanre, D., Buis, J. P., Setzer, A., Vermote, E., Reagan, J. A., Kaufman, Y. J., Nakajima, T., Lavenu, F., Jankowiak, I., and Smirnov, A. (1998). AERONET – a federated instrument network and data archive for aerosol characterization. *Remote Sens. Environ.*, 66:1–16.

Holzer-Popp, T., de Leeuw, G., Griesfeller, J., Martynenko, D., Klüser, L., Bevan, S., Davies, W., Ducos, F., Deuzé, J. L., Graigner, R. G., Heckel, A., von Hoyningen-Hüne, W., Kolmonen, P., Litvinov, P., North, P., Poulsen, C. A., Ramon, D., Siddans, R., Sogacheva, L., Tanré, D., Thomas, G. E., Vountas, M., Descloitres, J., Griesfeller, J., Kinne, S., Schulz, M., and Pinnock, S. (2013). Aerosol retrieval experiments in the ESA aerosol cci project. *Atmos. Meas. Tech.*, 6(8):1919–1957.

IPCC (2013). *Fifth Assessment Report: Climate Change 2013*. Cambridge University Press, New York, NY, USA.

Jacobson, M. (2001). Global direct radiative forcing due to multicomponent anthropogenic and natural aerosols. *J. Geophys. Res.*, 106(D2):1551–1568.

Järvi, L., Hannuniemi, H., Hussein, T., Junninen, H., Aalto, P., Hillamo, R., Mäkelä, T., Keronen, P., Siivola, E., Vesala, T., and Kulmala, M. (2009). The urban measurement station SMEAR III:continuous monitoring of air pollution and surfaceatmosphere interactions in helsinki, finland. *Boreal Env. Res.*, 14:1797–2469.

Jethva, H., Torres, O., Waquet, F., Chand, D., and Hu, Y. (2014). How do A-train sensors intercompare in the retrieval of above-cloud aerosol optical depth? A case study-based assessment. *Geophys. Res. Lett.*, 4(7):186–192.

Kahn, R. A. and Limbacher, J. (2012). Eyjafjallajökull volcano plume particle-type characterization from space-based multi-angle imaging. *Atmos. Chem. Phys.*, 12(20):9459–9477.

Kanawade, V., Tripathi, S., Siingh, D., Gautam, A., Srivastava, A., Kamra, A., Soni, V., and Sethi, V. (2014). Observations of new particle formation at two distinct indian subcontinental urban locations. *Atm. Environ.*, 96:370–379.

Klett, J. (1981). Stable analytical inversion solution for processing lidar returns. *Appl. Opt.*, 20(2):211–220.

Kokhanovsky, A. and de Leeuw, G. (2009). *Atmospheric Aerosols: Global Climatology and Radiative Characteristics*. Springer Verlag.

Kyrö, E.-M., Kerminen, V.-M., Virkkula, A., Dal Maso, M., Parshintsev, J., Ruíz-Jimenez, J., Forsström, L., Manninen, H. E., Riekkola, M.-L., Heinonen, P., and Kulmala, M. (2013). Antarctic new particle formation from continental biogenic precursors. *Atmos. Chem. Phys.*, 13(7):3527–3546.

Levy, R. C., Mattoo, S., Munchak, L. A., Remer, L. A., Sayer, A. M., Patadia, F., and Hsu, N. C. (2013). The collection 6 MODIS aerosol products over land and ocean. *Atmos. Meas. Tech.*, 6(11):2989–3034.

Liu, J., Mauzerall, D., and Horowitz, L. (2009). Evaluating inter-continental transport of fine aerosols:(2) global health impact. *Atm. Environ.*, 43:4339–4347.

Loeb, N. G. and Kato, S. (2002). Top-of-atmosphere direct radiative effect of aerosols over the tropical oceans from the clouds and the earth's radiant energy system (CERES) satellite instrument. *J. Climate*, 15:1474–1484.

Loeb, N. G. and Manalo-Smith, N. (2005). Top-of-atmosphere direct radiative effect of aerosols over global oceans from merged CERES and MODIS observations. *J. Climate*, 18:3506–3526.

Lohmann, U. and Feichter, J. (2005). Global indirect aerosol effects: a review. *Atmos. Chem. Phys.*, 5(3):715–737.

Lopatin, A., Dubovik, O., Chaikovsky, A., Goloub, P., Lapyonok, T., Tanré, D., and Litvinov, P. (2013). Enhancement of aerosol characterization using synergy of lidar and sun-photometer coincident observations: the GARRLiC algorithm. *Atmos. Meas. Tech.*, 6(8):2065–2088.

Ma, X., Yu, F., and Quaas, J. (2014). Reassessment of satellite-based estimate of aerosol climate forcing. *J. Geophys. Res.*, 119:1039410409.

Mäkelä, J., Dal Maso, M., Pirjola, L., Keronen, P., Laakso, L., Kulmala, M., and Laaksonen, A. (2000). Characteristics of the atmospheric particle formation events observed at a borel forest site in southern finland. *Boreal Env. Res.*, 5:299–313.

Mei, L., Xue, Y., de Leeuw, G., von Hoyningen-Huene, W., Kokhanovsky, A., Istomina, L., Guang, J., and Burrows, J. (2013a). Aerosol optical depth retrieval in the arctic region using MODIS data over snow. *Remote Sens. Environ.*, 128:234–245.

Mei, L., Xue, Y., Kokhanovsky, A., von Hoyningen-Huene, W., Istomina, L., de Leeuw, G., Burrows, J., Guang, J., and Jing, Y. (2013b). Aerosol optical depth retrieval over snow using AATSR data. *Int. J. Remote. Sens.*, 34(14):5030–5041.

Menon, S., Hansen, J., Nazarenko, L., and Luo, Y. (2002). Long-term impacts of aerosols on the vertical development of clouds and precipitation. *Science*, 297:888–894.

Mie, G. (1908). Beiträge zur optik trüber medien, speziell kolloidaler metallösungen. *Ann. Phys.*, 330:377–445.

Mishchenko, M. I. and Travis, L. D. (1998). Capabilities and limitations of a current FORTRAN implementation of the T-matrix method for randomly oriented, rotationally symmetric scatterers. *J. Quant. Spectrosc. Radiat. Transfer*, 60:309–324.

Pappalardo, G., Amodeo, A., Apituley, A., Comeron, A., Freudenthaler, V., Linné, H., Ansmann, A., Bösenberg, J., D'Amico, G., Mattis, I., Mona, L., Wandinger, U., Amiridis, V., Alados-Arboledas, L., Nicolae, D., and Wiegner, M. (2014). EARLINET: towards an advanced sustainable european aerosol lidar network. *Atmos. Meas. Tech.*, 7(8):2389–2409.

Patadia, F., Gupta, P., and Christopher, S. A. (2008). First observational estimates of global clear sky shortwave aerosol direct radiative effect over land. *Geophys. Res. Lett.*, 35(D02109).

Petty, G. W. (2006). *A First Course In Atmospheric Radiation*. Sundog Publishing.

Quaas, J., Boucher, O., Belloiun, N., and Kinne, S. (2008). Satellite-based estimate of the direct and indirect aerosol climate forcing. *J. Geophys. Res.*, 113(D05204).

Remer, L., Kleidman, R., Levy, R., Kaufman, Y., Tanre, D., Mattoo, S., Martins, J., Ichoku, C., Koren, I., Yu, H., and Holben, B. (2008). Global aerosol climatology from the MODIS satellite sensors. *J. Geophys. Res.*, 113(D14S07).

Schnelle-Kreis, J., Küpper, U., Sklorz, M., Cyrys, J., Briede, J., Peters, A., and Zimmerman, R. (2009). Daily measurements of organic compounds in ambient particulate matter in augsburg, germany: new aspects on aerosol sources and aerosol related health effects. *Biomarkers*, 14:39–44.

Schulz, M., Textor, C., Kinne, S., Balkanski, Y., Bauer, S., Berntsen, T., Berglen, T., Boucher, O., Dentener, F., Guibert, S., Isaksen, I. S. A., Iversen, T., Koch, D., Kirkevåg, A., Liu, X., Montanaro, V., Myhre, G., Penner, J. E., Pitari, G., Reddy, S., Seland, Ø., Stier, P., and Takemura, T. (2006). Radiative forcing by aerosols as derived from the AeroCom present-day and pre-industrial simulations. *Atmos. Chem. Phys.*, 6(12):5225–5246.

Schuster, G., Dubovik, O., and Holben, B. (2006). Angstrom exponent and bimodal aerosol size distributions. *J. Geophys. Res.*, 111(D07207).

Seaton, A., MacNee, W., Donaldson, K., and Godden, D. (1995). Particulate air pollution and acute health effects. *The Lancet*, 345:176–178.

Sena, E. T., Artaxo, P., and Correia, A. L. (2013). Spatial variability of the direct radiative forcing of biomass burning aerosols and the effects of land use change in Amazonia. *Atmos. Chem. Phys.*, 13(3):1261–1275.

Sofiev, M., Vankevich, R., Lotjonen, M., Prank, M., Petukhov, V., Ermakova, T., Koskinen, J., and Kukkonen, J. (2009). An operational system for the assimilation of the satellite information on wild-land fires for the needs of air quality modelling and forecasting. *Atmos. Chem. Phys.*, 9(18):6833–6847.

Spracklen, D. V., Carslaw, K. S., Merikanto, J., Mann, G. W., Reddington, C. L., Pickering, S., Ogren, J. A., Andrews, E., Baltensperger, U., Weingartner, E., Boy, M., Kulmala, M., Laakso, L., Lihavainen, H., Kivekäs, N., Komppula, M., Mihalopoulos, N., Kouvarakis, G., Jennings, S. G., O'Dowd, C., Birmili, W., Wiedensohler, A., Weller, R., Gras, J., Laj, P., Sellegri, K., Bonn, B., Krejci, R., Laaksonen, A., Hamed, A., Minikin, A., Harrison, R. M., Talbot, R., and Sun, J. (2010). Explaining global surface aerosol number concentrations in terms of primary emissions and particle formation. *Atmos. Chem. Phys.*, 10(10):4775–4793.

Sundström, A.-M., Nikandrova, A., Atlaskina, K., Nieminen, T., Vakkari, V., Laakso, L., Beukes, J. P., Arola, A., van Zyl, P. G., Josipovic, M., Venter, A. D., Jaars, K., Pienaar, J. J., Piketh, S., Wiedensohler, A., Chiloane, E. K., de Leeuw, G., and Kulmala, M. (2014). Characterization of satellite based proxies for estimating nucleation mode particles over south africa. *Atmos. Chem. Phys. Discuss.*, 14(18):25825–25867.

Thomas, G. E., Chalmers, N., Harris, B., Grainger, R. G., and Highwood, E. J. (2013). Regional and monthly and clear-sky aerosol direct radiative effect (and forcing) derived from the globAEROSOL-AATSR satellite aerosol product. *Atmos. Chem. Phys.*, 13(1):393–410.

Toledano, C., Bennouna, Y., Cachorro, V., Ortiz de Galisteo, J., Stohl, A., Stebel, K., Kristiansen, N., Olmo, F., Lyamani, H., Obregon, M., Estelles, V., Wagner, F., Baldasano, J., Gonzalez-Castanedo, Y., Clarisse, L., and de Frutos, A. (2012). Aerosol properties of the Eyjafjallajökull ash derived from sun photometer and satellite observations over the Iberian Peninsula. *Atm. Environ.*, 48:22–32.

Torres, O., Jethva, H., and Bhartia, P. (2012). Retrieval of aerosol optical depth above clouds from OMI observations: Sensitivity analysis and case studies. *J. Atmos. Sci.*, 69:1037–1053.

Utell, M. and Frampton, M. (2000). Health effects of ambient air pollution: The ultrafine particle hypothesis. *J. Aerosol Med. Pulm. Drug Deliv.*, 13(4):355–359.

Vakkari, V., Laakso, H., Kulmala, M., Laaksonen, A., Mabaso, D., Molefe, M., Kgabi, N., and Laakso, L. (2011). New particle formation events in semi-clean south african savannah. *Atmos. Chem. Phys.*, 11(7):3333–3346.

Virtanen, T. H., Kolmonen, P., Rodríguez, E., Sogacheva, L., Sundström, A.-M., and de Leeuw, G. (2014). Ash plume top height estimate using AATSR. *Atmos. Meas. Tech.*, 7(4):3863–3913.

Wadinger, U. (2005). Introduction to Lidar. In Weitkamp, C., editor, *Lidar: Range-Resolved Optical Remote Sensing of the Atmosphere*. Springer Science.

Wang, Z. B., Hu, M., Sun, J. Y., Wu, Z. J., Yue, D. L., Shen, X. J., Zhang, Y. M., Pei, X. Y., Cheng, Y. F., and Wiedensohler, A. (2013). Characteristics of regional new particle formation in urban and regional background environments in the north china plain. *Atmos. Chem. Phys.*, 13(24):12495–12506.

WHO (2005). *WHO Air quality guidelines for particulate matter, ozone, nitrogen dioxide and sulfur dioxide. Global Update 2005, Summary of risk assesment*. World Health Organization.

Winker, D., Hunt, W., and McGill, M. (2007). Initial performance assessment of CALIOP. *Geophys. Res. Lett.*, 34(L19803).

YTV (2007). *Air Quality in the Helsinki Metropolitan Area*. YTV Helsinki Metropolitan Area Council.

Zhang, J., Reid, J., Westphal, D., Baker, N., and Hyer, E. (2008). A system for operational aerosol optical depth data assimilation over global oceans. *J. Geophys. Res.*, 113(D10208).

Zhao, T., Yu, H., Laszlo, I., Chin, M., and Conant, W. (2008). Derivation of component aerosol direct radiative forcing at the top of the atmosphere for clear-sky oceans. *J. Quant. Spectrosc. Radiat. Transfer*, 109:1162–1186.